Cellular/Molecular

Periodic Organization of a Major Subtype of Pyramidal Neurons in Neocortical Layer V

Hisato Maruoka, Kazumasa Kubota, Rumi Kurokawa, Shun Tsuruno, and Toshihiko Hosoya
RIKEN Brain Science Institute, Wako, Saitama 351-0198, Japan

A major question in neocortical research is the extent to which neuronal organization is stereotyped. Previous studies have revealed functional clustering and neuronal interactions among cortical neurons located within tens of micrometers in the tangential orientation (orientation parallel to the pial surface). In the tangential orientation at this scale, however, it is unknown whether the distribution of neuronal subtypes is random or has any stereotypy. We found that the tangential arrangement of subcerebral projection neurons, which are a major pyramidal neuron subtype in mouse layer V, was not random but significantly periodic. This periodicity, which was observed in multiple cortical areas, had a typical wavelength of 30 μm. Under specific visual stimulation, neurons in single repeating units exhibited strongly correlated c-Fos expression. Therefore, subcerebral projection neurons have a periodic arrangement, and neuronal activity leading to c-Fos expression is similar among neurons in the same repeating units. These results suggest that the neocortex has a periodic functional micro-organization composed of a major neuronal subtype in layer V.

Introduction

One of the major questions in neocortical research is the extent to which neuronal organization is stereotyped (Silberberg et al., 2002), because stereotypy suggests that identical circuit mechanisms are used repeatedly. In particular, stereotypy in the organization of functional subtypes of neurons shapes the basic structure of cortical circuits. One example is the stereotyped distribution of neuronal subtypes across cortical layers. In contrast, stereotypy in the orientation parallel to the pial surface, i.e., in the tangential orientation, is not well understood.

Previous studies have revealed functional clustering and neuronal interactions among cortical neurons located within tens of micrometers in the tangential orientation. For example, functional clustering at this scale is observed in the visual and motor cortex (Hubel and Wiesel, 1974, 1977; Ohki et al., 2006; Georgopoulos et al., 2007; Dombeck et al., 2009; Kara and Boyd, 2009). In rodent neocortical layer II/III, the probability of connection between pyramidal neurons located within tens of micrometers in the tangential orientation is higher than that between those located further apart (Holmgren et al., 2003). In addition, temporal correlation of neuronal activity is higher for neurons located within tens of micrometers in the tangential orientation than for those located further apart (Dombeck et al., 2009; Komiyama et al., 2010). These observations suggest important roles of cortical circuits at the scale of tens of micrometers in the tangential orientation. At this scale in the tangential orientation, however, it is unknown whether the organization of neuronal subtypes is random or has any stereotypy.

Mouse neocortical layer V has two major classes of pyramidal neurons: subcerebral and callosal projection neurons (Molnár and Cheung, 2006; Molyneaux et al., 2007). Subcerebral projection neurons project to targets outside the neocortex, such as the superior colliculus or spinal cord, whereas callosal projection neurons project to the neocortex in the opposite hemisphere. Marker genes including *COUP TF-interacting protein 2* (*ctip2*) and μ-crystallin (*crym*) are specifically expressed in subcerebral projection neurons (Arlotta et al., 2005; Molnár and Cheung, 2006; Molyneaux et al., 2007).

inhibitor of DNA binding 2 (*id2*), which encodes a basic helix-loop-helix transcriptional inhibitor (Lasorella et al., 2006; Kee, 2009), is expressed in layer V as well as in layers II/III and VI (Neuman et al., 1993; Rubenstein et al., 1999). In layer V of the P6 mouse visual cortex, cells expressing *id2* mRNA form column-like clusters (Rubenstein et al., 1999). These clusters are surrounded by *id2*(−) cells, and multiple clusters are located tangentially. Therefore, *id2*(+) cells may have a nonrandom tangential distribution.

We investigated whether any neuronal subtypes have stereotyped tangential organization at the scale of tens of micrometers. In layer V, *id2* was specifically expressed in subcerebral projection neurons. Subcerebral projection neurons had a periodic tangential arrangement with a typical wavelength of 30 μm. Under specific visual stimulation, neurons in a single repeating unit exhibited highly correlated c-Fos expression. Therefore, subcerebral projection neurons have a stereotyped, periodic tangential organization at the scale of tens of micrometers and neuronal activity leading to c-Fos expression is similar within single repeating units.

Received June 19, 2011; revised Oct. 10, 2011; accepted Nov. 3, 2011.

Author contributions: T.H. designed research; H.M., K.K., R.K., and S.T. performed research; H.M., R.K., S.T., and T.H. analyzed data; T.H. wrote the paper.

This work was supported by research funds from RIKEN and a Grant-in-Aid for Scientific Research on Innovative Areas "Mesoscopic Neurocircuitry" (22115004) from the Ministry of Education, Culture, Sports, Science and Technology of Japan. We thank Drs. Noritaka Ichinohe, Kathleen S. Rockland, Yoshiyuki Kubota, Mieko Morishima, Kenichi Ohki, Jeffrey D. Macklis, H. Sebastian Seung, Charles T. Yokoyama, and Nirao Shah for reviewing this manuscript and the BSI-Olympus Collaboration Center for their assistance regarding microscopy.

This article is freely available online through the *J Neurosci* Open Choice option.

Correspondence should be addressed to Dr. Toshihiko Hosoya, RIKEN Brain Science Institute. Hirosawa 2-1, Wako, Saitama 351-0198, Japan. E-mail: hosoya@brain.riken.jp.

DOI:10.1523/JNEUROSCI.3117-11.2011

 0270-6474/11/3118522-21$15.00/0

Materials and Methods

Mice. All experiments were approved by RIKEN committees (Wako Animal Experiments Committee and Genetic Recombinant Experiment Safety Committee) and were performed in accordance with the institutional guidelines of the animal facilities of RIKEN-BSI. C57BL/6J and ICR mice were purchased from Japan SLC. Z/EG mice (Novak et al., 2000) were obtained from the Jackson Laboratory. *Crym*-BAC-EGFP transgenic mice were obtained from the GENSAT BAC Transgenic Project (www.gensat.org) and maintained as heterozygous animals with the C57BL/6J genetic background. The BLBP promoter (−1547 to +72) (Feng and Heintz, 1995; Anthony et al., 2004) and *Cre-ER* sequence (Danielian et al., 1998) were obtained by PCR using genomic DNAs of C57 BL/6 and *CAGGCre-ER* mice (The Jackson Laboratory) (Hayashi and McMahon, 2002), respectively, as templates. The two fragments were subcloned into the upstream region of the β-globin polyA cassette in the pBI Tet vector (BD Biosciences). *BLBP-Cre-ER* transgenic mice were generated using standard protocols.

Retrograde labeling. Neonatal mice at P2 (for double staining for Id2 protein) and adult mice at P21–76 [for double staining for the enhanced green fluorescent protein (EGFP)] were anesthetized with ice and sodium pentobarbital (60 mg/kg body weight, injected intraperitoneally), respectively. When adult mice were being injected, a small craniotomy was created to expose the injection sites. Cholera toxin subunit B conjugated with AlexaFluor 488 or 594 (1–5 mg/ml in PBS, Invitrogen) was injected using a glass micropipette. To label subcerebral projection neurons, tracers were injected into the pons-midbrain junction. To label callosal projection neurons, the injection was administered to the contralateral visual or somatosensory cortex at three sites along the rostrocaudal axis. At each injection site in the contralateral cortex, the injection was administered while advancing the micropipette perpendicularly to the pial surface to a depth of ~1.0 mm. Two days after the injection, perfusion was performed as described below. Strongly labeled slices were further stained for protein expression.

Tamoxifen administration. Z/EG female mice were mated with *BLBP-Cre-ER* male mice and checked for vaginal plugs from 8:00 A.M. to 9:30 A.M. If vaginal plugs were detected, 12:00 A.M. on that day was counted as embryonic day 0 (E0). 4-Hydroxytamoxifen (Sigma H7904) was solubilized in H_2O using the Hydrophobic Drug Solubilization kit (Purebright SL-310, NihonYushi) and diluted to a concentration of 0.5–1.5 mg/ml with 0.9% NaCl (aq) (typically 1:6–1:30). The tamoxifen solution (300–400 μl) was intraperitoneally injected into pregnant mice. The time (E11.5) and amount (20 mg/kg body weight) of tamoxifen administration was determined as below. Since pups were often eaten by injected mothers, they were delivered by Caesarean section and fed by foster mothers. Pups were perfused at P4 and those carrying the two transgenes were identified by genomic PCR.

The time of tamoxifen administration was adjusted so that the method generated clusters of progeny neurons that (1) originated from single cortical progenitor cells and (2) included layer V neurons. When tamoxifen was administered at 5 mg/kg body weight at E11.5, EGFP(+) cells were found in five of 18 newborn mice carrying the two transgenes. In these five mice, EGFP(+) cells formed six radial clusters (0.33 clusters per animal). This low probability of generation of clusters suggests that each cluster was generated by a single chromosomal excision event in a single cortical progenitor cell. All cells in these clusters had a pyramidal shape. Even though the clusters were rare, all of them contained layer V cells. Therefore it was decided that tamoxifen should be administered at E11.5.

To perform simultaneous labeling of EGFP(+) clusters and *id2* mRNA, it was necessary to increase the number of EGFP(+) clusters per mouse. For this purpose, the drug concentration was increased to 20 mg/kg body weight. Under this high-dose condition, 52 EGFP(+) clusters, all comprising neurons with a pyramidal cell shape, were found among 11 pups carrying the two transgenes. Thus, as expected, the number of clusters per animal was increased (4.73 clusters per animal). Despite this increased number of clusters, the characteristics of single clusters under high-dose conditions were similar to those under low-dose conditions: (1) the number of EGFP(+) cells in single clusters were similar between the two conditions [low-dose: 63.3 ± 11.4 (mean ± SD), $n = 6$ clusters; high-dose: 68.7 ± 24.7 (mean ± SD), $n = 52$ clusters; $p > 0.5$, two-tailed bootstrap test], and (2) under both conditions, the clusters showed similar spatial distributions (the diameter of clusters was 100–150 μm in layer V and 200–300 μm in layer II/III). Therefore, similar to clusters generated under the low-dose condition, clusters generated under the high-dose condition most probably comprised neurons generated by single cortical progenitor cells. Therefore, it was decided that tamoxifen should be administered at 20 mg/kg body weight at E11.5.

Single-eye visual stimulation. Crym-BAC-EGFP transgenic mice (P28–47) were anesthetized with sodium pentobarbital (60 mg/kg body weight, injected intraperitoneally). Right eyelids of the mice were carefully trimmed and sutured with 6–0 sterile surgical silk (Natsume Seisakusyo). After recovery, the mice were placed in total darkness overnight. The mice were then transferred to a white cylindrical container (diameter 30 cm, height 36 cm) and illuminated for 2 h with a white fluorescent light (1800 lm) placed on top of the container.

Perfusion. Mice were deeply anesthetized with diethyl ether or sodium pentobarbital and perfused transcardially with ice-cold 0.9% saline, followed by fixation with 4% paraformaldehyde (PFA) in 0.1 M phosphate buffer (PB). After the brains were dissected, they were further fixed with PFA overnight at 4°C and then incubated in 30% sucrose in 0.1 M PB overnight at 4°C. Free-floating slices were prepared using linear slicers (PRO7, Dosaka EM, and ROM 670e, Yamato Kohki Kougyou).

Immunohistochemistry. Primary antibodies used were as follows: anti-GFP rat monoclonal antibody (Nacalai Tesque, GF090R, 1:1000), anti-GFP rabbit polyclonal antibody (Invitrogen, A6455, 1:1000), anti-Id2 (C-20) rabbit polyclonal antibody (Santa Cruz Biotechnology, sc-489, 1:250), and anti-c-Fos rabbit polyclonal antibody (Santa Cruz Biotechnology, sc-52, 1:1000). Free-floating slices were permeabilized with a solution containing 10% normal goat serum (NGS), 0.2% bovine serum albumin, and 0.1% Triton X-100 in 0.1 M PBS for 2 h at 37°C and incubated in the same solution containing primary antibodies overnight at 25°C. After washing with 0.1 M PBS, the slices were incubated with secondary antibodies conjugated with AlexaFluor 488 or 594 (Invitrogen, 1:500) and DAPI (4′,6-diamidino-2-phenylindole, Invitrogen, 1:5000) for nuclear staining for 2 h at 25°C. Finally, the slices were mounted on glass slides and embedded in ProLong Gold Antifade Reagent (Invitrogen).

In situ *hybridization for mRNA.* cDNA fragments of the marker genes were obtained by PCR using cDNA libraries of mouse E17 embryos and the mouse brain (QUICK-Clone cDNA, Clontech) as templates. The primer sequences are listed as follows: *id2* (NCBI No. NM_010496) forward (F): 5′–3′ CGAGCAGCATGAAAGCCTTCAGTCCGGTGA; reverse (R): CTGGGTCCTCCTGGAATTCACGCTCCACCT; *ctip2* (NM_021399) F: CACCTGTGGCCAGTGTCAGATGAACTTCCC; R: TGCGTCTTCATGTGGCGCTTGAGCTTGCTC; *lmo4* (NM_010723) F: TGTTGCAATATAGGGGAGAAGCAGACCATGGTGAAT; R: ACAAACCTTCTGGTCTGGCAGTAGTGGATT; *crym* (NM_016669) F: AGCGCAGAGGAGGTGCAGGATCACCTT; R: TGAGATCTTCACAGAGCAGTTCTCCTTCAA. After subcloning into the pCRII-TOPO vector (Invitrogen), these fragments were used as templates for *in vitro* transcription to synthesize digoxigenin (DIG)- and fluorescein isothiocyanate (FITC)-labeled riboprobes (DIG-labeling kit and FITC RNA LabelingMix, Roche Diagnostics).

Free-floating slices were fixed with 4% PFA for 1 h at 25°C or overnight at 4°C, treated twice with glycine (0.75% in 0.1 M PB, pH 8.0) for 15 min at 25°C and Triton X-100 (0.3% in 0.1 M PB, pH 8.0) for 15 min at 25°C, acetylated by incubating in 0.25% acetic anhydride in 0.1 M triethanolamine, pH 8.0, for 10 min at 25°C, and then incubated in hybridization buffer [5× standard saline citrate (SSC), 50% formamide, 2% Blocking Reagent (Roche Diagnostics), 0.1% *N*-lauroylsarcosine, 0.1% SDS] containing 1–10 μg/ml riboprobes for 15 h at 60°C–64°C. A DIG-labeled riboprobe was used for detection with the NBT/BCIP reaction, whereas two riboprobes, one DIG-labeled and one FITC-labeled, were used for double fluorescent *in situ* hybridization (FISH).

After hybridization, slices were sequentially treated as follows: twice with 2× SSC/50% formamide/0.1% *N*-lauroylsarcosine for 15 min at 50°C–60°C; twice with RNase buffer (10 mM Tris-HCl, pH 8.0, 10 mM EDTA, 500 mM NaCl) containing 20 μg/ml RNase A (Sigma) for 15 min

at 37°C; twice with 2× SSC/0.1% *N*-lauroylsarcosine for 15 min at 37°C; and twice with 0.2× SSC/0.1% *N*-lauroylsarcosine for 15 min at 37°C. The slices were then treated differently for the two detection methods.

For detection with the NBT/BCIP reaction, slices were blocked in the blocking buffer (1% Blocking Reagent, 1 M Tris-HCl, pH 7.5, 0.5 M EDTA) for 1 h at 25°C and incubated in the blocking buffer containing anti-DIG-alkaline phosphatase (Roche Diagnostics, 1:1000) for 18 h at 4°C. After washing the slices three times in TNT (0.1 M Tris-HCl, pH 7.5, 0.15 M NaCl, 0.05% Tween 20) for 15 min at 25°C and once in 0.1 M Tris-HCl (pH 9.5)/0.1 M NaCl/50 mM $MgCl_2$ for 5 min at 25°C, alkaline phosphatase activity was detected using the NBT/BCIP detection set (Roche Diagnostics). The reaction was stopped by washing the slices four times in PBS containing 0.5 mM EDTA.

For double FISH, slices were incubated in the blocking buffer containing anti-FITC antibody conjugated with horseradish peroxidase (Roche Diagnostics, 1:1500–1:2000) for 18 h at 4°C. The slices were washed three times in TNT for 15 min at 25°C and treated with the TSA Plus DNP reagent (1:50, PerkinElmer) for 10–30 min at 25°C. After washing twice in TNT for 5 min at 25°C and once in 0.1 M Tris-HCl (pH 7.5)/15 mM EDTA for 5 min at 25°C, the slices were blocked for 1 h at 25°C and incubated in anti-DIG-alkaline phosphatase for 18 h at 4°C as described above. The slices were then incubated with anti-DNP antibody conjugated with AlexaFluor 488 (Roche Diagnostics, 1:500) in the blocking buffer for 1–2 h at 25°C. After washing three times in TNT for 15 min at 25°C and once in 0.1 M Tris-HCl (pH 8.0)/0.1 M NaCl/10 mM $MgCl_2$ for 5 min at 25°C, alkaline phosphatase activity was detected using an HNPP fluorescence detection set (Roche Diagnostics). The slices were incubated for 30 min and then washed in PBS containing 0.5 mM EDTA. The slices were counterstained with TOTO-3 (Invitrogen, 1:500) in 0.1 M PBS for 15–20 min or with DAPI (1:2000 in PBS).

Simultaneous detection of mRNA and EGFP protein. For simultaneous detection of mRNA and EGFP protein, free-floating slices were postfixed in 4% PFA for 90 min at 25°C; washed twice in 0.1 M PB; blocked in a solution containing 3% NGS, 0.05–0.25% Triton X-100, and 0.1 M PBS for 1–2 h at 25°C; and incubated in the same solution containing anti-GFP antibody (1:1000) and RNase inhibitor (TOYOBO, 1:500) for 15 h at 4°C. After washing three times with 0.1 M PB, the slices were incubated in a solution containing 3% NGS, 0.05%–0.25% Triton X-100, 0.1 M PBS, biotinylated secondary IgG (Vector Laboratories, 1:500), and RNase inhibitor for 3 h at 25°C. The slices were washed three times in 0.1 M PB, postfixed with 4% PFA for 30 min at 25°C, and processed for *in situ* hybridization with DIG-labeled riboprobes as described above. After incubation with anti-DIG-alkaline phosphatase, the slices were incubated in 1.0% blocking buffer containing streptavidin-Alexa 488 (1:500) for 30–120 min at 25°C. Alkaline phosphatase activity was detected using the HNPP fluorescence detection set as described above.

Slice preparation. To prepare parasagittal slices of the posterior visual cortex of P4 mice for the analysis of periodicity, the cutting plane (see Fig. 2*D*, red line) was tilted by 4–8° from the median plane (see Fig. 2*D*, black line). The thickness of the slices was 30 μm. Slices were stained for *id2* mRNA by FISH. In Figure 2*E*, stained slices are aligned in the lateral-to-medial order. In the posterior ventral part of these slices, *id2*(+) cells formed two layers (see Fig. 2*E*, open and solid circles). In medial slices (Fig. 2*E*4), the two layers are closer to each other (see Fig. 2*E*4, open circle) compared with those in lateral slices (see Fig. 2*E*1–*E*3, solid circles). These medial slices were not analyzed. Among the remaining slices (Fig. 2*E*1–*E*3), those from medial positions (Fig. 2*E*2,*E*3) showed a sudden change of orientation in the upper layers of *id2*(+) cells (see Fig. 2*E*2,3, solid arrowheads), whereas those from more lateral positions (Fig. 2*E*1) did not show such sudden changes (see Fig. 2*E*1, open arrowhead). The former slices (Fig. 2*E*2,*E*3) were used for analysis. Approximately 600–700 μm layer V shown by boxes in Figure 2*F* was analyzed.

To analyze periodic arrangement in coronal slices of the somatosensory cortex of P9 mice, the cutting plane was tilted from the coronal plane by ~4° in the anterior direction (see Fig. 4*D*). The thickness of the slices was 34 μm. Slices were stained for *id2* mRNA with the NBT/BCIP reaction. In Figure 4*E–H*, stained slices are aligned in the anterior-to-posterior order. Slices that were anterior to the hippocampus (Fig. 4*E*1–*G*1) were selected, and those that contained the hippocampus (Fig. 4*H*1) were not analyzed. Because the medial-lateral extent of *id2* expression gradually changed depending of the anterior–posterior position in the brain (Rubenstein et al., 1999), among the selected slices (Fig. 4*E*1–*G*1), anterior slices showed strong *id2* mRNA expression in layer V of a relatively lateral part in the cortex (see Fig. 4*E*1), whereas posterior slices (Fig. 4*F*1, *G*1) showed strong *id2* mRNA expression in layer V of more medial parts in the cortex. Arrows in Figure 4*E*1–*G*1 mark the positions from which strong *id2* expression extended laterally. Slices in which these positions were more medial than the center of the hemisphere (see Fig. 4*E*1–*G*1, dashed line) were analyzed. Therefore, among these four slices, those shown in Figure 4 *F* and *G* were used for the analysis. Approximately 1100 μm layer V extending laterally from the arrow was analyzed.

Crym-BAC-EGFP brain slices containing EGFP(+) cells in the binocular region were prepared as follows. Single-eye visual stimulation was applied to the left eye of *Crym*-BAC-EGFP mice (see above). After perfusion, a small cut was made on the right hemisphere to discriminate between the left and right hemispheres. Brains were sliced (thickness of 30 μm) into the orientation shown by the purple line in Figure 7*F* and then stained for EGFP and c-Fos proteins. The binocular region was located by c-Fos expression in the left visual cortex. Among slices that showed c-Fos expression in the binocular region, those that contained EGFP(+) cells in layer V in the binocular region were selected. In *Crym*-BAC-EGFP mice, EGFP expression in layer V was not uniform in the anterior–posterior orientation of the visual cortex (see Fig. 7*G*). In layer V of the binocular region, EGFP was expressed only ~200 μm in the anterior–posterior orientation (see Fig. 7*G*, asterisk). Consistently, typically 4–6 slices per animal contained EGFP(+) cells in layer V in the binocular region. In these slices, the distribution of c-Fos(+) cells was asymmetric between the left and right hemispheres in a manner consistent with the anatomy of the visual pathway from single eyes. In the hemisphere contralateral to the stimulated eye, c-Fos was expressed across ~1200 μm in the tangential orientation (see Fig. 7*H*, left), whereas in the hemisphere ipsilateral to the stimulated eye (see Fig. 7*H*, right), c-Fos expression was limited to ~600 μm. Because the density of c-Fos(+) cells was higher in layers IV and VI than in layer V in the binocular region, the tangential range of the binocular region was determined by locating the tangential limits of c-Fos expression in layers IV and VI. The c-Fos expression was driven by the visual stimulus because (1) it was asymmetric as expected from the anatomy of the visual pathway and (2) virtually no c-Fos expression was observed in the visual cortex of mice kept in the dark (data not shown).

When preparing slices for other purposes, the slicing planes were parallel to the median plane (see Fig. 2*D*, black line) or to the coronal plane (see Fig. 4*D* and Fig. 7*F*, black lines). The thickness of these slices is described in the legends.

Microscopy. Digital images were captured using the BZ8000 fluorescence microscope (Keyence), IX81-ZDC epifluorescence microscope equipped with EM-CCD camera (Olympus), and Fluoview FV1000-D confocal laser scanning microscope (Olympus). Linear intensity adjustment was applied on each color channel.

Cell positions. Figure 3 illustrates periodicity analysis performed on the slice shown in Figure 2*H*. The two-dimensional coordinates of labeled cells were determined on photographs (see Fig. 3*A*1). In FISH experiments, nuclear staining images were used to determine the positions of labeled cells by locating their nuclei.

Cell positions relative to the center line of layer V. In the analysis of layer V of the posterior visual cortex in P4 mice, cell positions were measured relative to the center line of layer V (see Fig. 3*A*1,*A*2) because layer V in this area is curved. The center line of layer V (see Fig. 3*A*1) was drawn by fitting a three- or four-knot spline to the positions of *id2*(+) cells in layer V. The fit was performed by mean-squared-error fitting. From each cell, a straight line was drawn perpendicular to the center line (see Fig. 3*A*1). The length of the straight line was defined as the radial position of the cell. The sign was determined based on the side of the cell according to the center line. The tangential position of the cell was determined by measuring the position of the base of the straight line along the center line from an arbitrary point on the center line. Figure 3*A*2 illustrates the positions of the marked *id2*(+) cells in Figure 3*A*1 measured relative to the center line of layer V.

In the analysis of the P9 somatosensory cortex and the adult visual cortex, periodicity analysis was performed with raw coordinates of cell positions because layer V was nearly straight. The center line of layer V was determined by fitting a straight line to the cell positions.

Histogram of relative positions. The histogram of relative positions was generated as follows (see Fig. 3*A*3). In the analysis of the P4 posterior visual cortex, cell positions relative to the center line of layer V (see Fig. 3*A*2) were used, whereas in the analysis of the P9 somatosensory cortex and the adult visual cortex, raw coordinates were used. *N* represents the number of all labeled cells. First, one cell among *N* cells was selected as a reference cell, and all cells were moved in parallel so that the reference cell was located on the origin (vertical line). The positions of $N-1$ cells other than the reference cell were plotted (see Fig. 3*A*3, top plane). The same process was repeated *N* times by selecting different cells as reference cells (see Fig. 3*A*3, the second and third plane). Finally, all $(N-1) \times N$ positions were plotted on the same plane (see Fig. 3*A*3, the bottom plane). The result was smoothed by convolving with the two-dimensional Gaussian function $z = \exp[-0.5 \times (x^2 + y^2)/\sigma^2]$ (see Fig. 3*A*4). σ is described in the figure legends.

Power spectrum and orientation of periodicity. To calculate the power spectrum of cell positions, cell positions relative to the center line of layer V were used for the P4 posterior visual cortex, and raw coordinates were used for the P9 somatosensory cortex and the adult visual cortex. Bins of 1 μm in width were aligned into an orientation (see Fig. 3*A*2, gray lines). The number of bins was typically 600 for the P4 visual cortex and 1100 for the P9 somatosensory and the adult visual cortices. The cell position histogram was generated by counting the number of labeled cells in these bins. The histogram for the cell positions in Figure 3*A*2 prepared with the bins in Figure 3*A*2 had clusters separated by spaces (see Fig. 3*A*5), suggesting a nonuniform distribution. The power spectrum was calculated by fast Fourier transformation. The power spectrum calculated for the cell position histogram in Figure 3*A*5 had a sharp peak (see Fig. 3*A*6), suggesting periodicity.

To quantify the strength of periodicity, the area below the power spectrum within a limited wavelength range was measured (see Fig. 3*A*6, red); this area is proportional to the variance of the wavelength components in the cell position histograms. For the slice shown in Figure 3*A*, because the peak wavelength in the power spectrum was ~25 μm (see Fig. 3*A*6), the wavelength range of 22.5–27.5 μm was used (see Fig. 3*A*6, red). This area was divided by the area between 10–150 μm to obtain the normalized power. The Kaiser window ($\beta = 3.14$) was used in calculating the normalized power.

The calculation of the normalized power was repeated while rotating the orientation of bins in increments of 1°, and the results were smoothed across orientations using a median filter that extended 5° (see Fig. 3*A*7). The range of rotation was as follows: in the P4 visual cortex, 0° to −30° relative to the center line of layer V, where the positive angle is in counterclockwise direction in Figure 3*A*2; in the P9 somatosensory cortex and the adult visual cortex, −15° to 15° relative to the center line of layer V. The orientation that resulted in the largest normalized power was defined as the orientation of periodicity. In Figure 3*A*7, the orientation of periodicity was −16° (see Fig. 3*A*7, thick red line), and the normalized power was 0.23. The power spectrum prepared for the orientation of periodicity is shown in Figure 3*A*8.

Statistical significance of periodicity. To examine the statistical significance, it was investigated how often the observed normalized power would be obtained if the cell distribution was random. For this purpose, $N = 1000$ or 10,000 surrogate datasets in which cells were randomly distributed were generated and analyzed as described above (see Fig. 3*B*).

To generate surrogates, the three-dimensional space in which cells were distributed was determined; this space had the same two-dimensional area as that of real cells (see Fig. 3*B*1, gray polygon) and the same thickness as the slice. Surrogates were generated by randomly locating cells (same number as the real cells) within the three-dimensional space (see Fig. 3*B*2, left). To avoid two cells having the same position, surrogates were discarded if any two cells were closer than 5 μm because in the real data, the minimal distance between the centers of two nuclei was ~5 μm (see Fig. 2*C*1). In the analysis of the P4 posterior visual cortex, surrogate cell positions were measured relative to the center line of layer V (see Fig. 3*B*2, right). In the analysis of the P9 somatosensory cortex and the adult visual cortex, raw coordinates of surrogates were used.

For each surrogate, the orientation of periodicity was determined (see Fig. 3*B*3, thick black lines) and the normalized power was measured. After performing analysis on all surrogates, the histogram of normalized power of the surrogates was generated (see Fig. 3*B*4, black line). The result was compared with the normalized power of the real data measured in the orientation of periodicity (see Fig. 3*B*4, red arrow). If *M* among the *N* surrogates had normalized power higher than that of the real data, the significance *P* was determined as $P = M/N$. In Figure 3*B*, among $N = 1000$ surrogates, only $M = 1$ had normalized power higher than that reported in the real data (see Fig. 3*B*4), and therefore $p = 0.001$.

An identical analysis was performed on all slices generated under the same slice preparation conditions described above. Because the peak wavelengths were slightly different among slices, we examined two wavelength ranges: in the P4 visual cortex, 20–25 μm and 22.5–27.5 μm; in the P9 somatosensory cortex, 30–35 μm and 32.5–37.5 μm; and in the adult visual cortex, 27.5–30.5 μm and 33–37 μm. If a slice had $p < 0.01$ for either of the two wavelength ranges, even in the worst case, the probability of $p < 0.01$ for either of the two wavelength ranges was $p = 0.02$. If *K* of *L* slices had significance smaller than $p < 0.01$ for either of the two wavelength ranges, the total significance P_{Total} was obtained by calculating the probability of having *K* or more significant slices under the random distribution, as follows:

$$P_{\text{Total}} = \sum_{i=K}^{L} {}_L C_i \, 0.02^i \, (1 - 0.02)^{L-i}. \quad (1)$$

Autocorrelogram. The autocorrelogram of cell positions was generated using cell positions relative to the center line of layer V for the P4 posterior visual cortex, and using raw coordinates for the P9 somatosensory cortex and the adult visual cortex. First, one cell was selected as a reference cell (see Fig. 3*C*1, red circle). A bin perpendicular to the orientation of periodicity was placed at a position with a distance measured along the orientation of periodicity (see Fig. 3*C*1). The number of cells in the bin was counted. The same process was repeated by selecting all cells as reference cells, except if the bin was outside the analyzed area. Data from both sides were merged, and the average number of cells in the bin was calculated. The same process was repeated for different distances to generate the autocorrelogram. The result was divided by the width of the bin such that the number of cells per micrometer was represented (see Fig. 3*C*2).

Autocorrelograms were also calculated for surrogate data. For each position, the highest 2.5%, the highest 15.9%, the median, the lowest 15.9%, and the lowest 2.5% of autocorrelograms calculated for surrogates were determined and shown by gray lateral lines (see Fig. 3*C*2).

Sensitivity and reliability of the periodicity analysis. The sensitivity and reliability of the periodicity analysis was evaluated by simulation (see Fig. 9). First, to evaluate the sensitivity, the periodicity analysis was performed on simulated cells that had periodic distribution. These cells were distributed similarly to EGFP(+) cells in layer V in Figure 8*A*. Eighty-six cells [same in number as EGFP(+) cells in layer V in Fig. 8*A*] were distributed in an area similar to that in layer V in Figure 8*A*, i.e., 150 and 1100 μm in the radial and tangential orientation, respectively. The cells were randomly distributed in the radial orientation, whereas in the tangential orientation, they were distributed according to a periodic distribution with a wavelength of 29.0 μm (similar to the wavelength measured for Fig. 8*A*). To distribute cells according to a periodic distribution, cells were first randomly located in the tangential orientation, then retained or removed according to a sinusoidally modulated probability. For example, in the sinusoid shown in Figure 9*A*1, probabilities at the peaks and troughs are 1 and 1/7, respectively. Accordingly, cells located at tangential positions where the probability curve had peaks were always retained, whereas those located at tangential positions where the probability curve had troughs were retained only once in seven cases. This process was repeated until the desired number of cells was generated. Figure 9*A*2 is an example set of cell positions determined by the process. Note that periodicity is not apparent.

Despite this lack of apparent periodicity, the periodicity analysis detected significant periodicity with the wavelength range of 27.5–30.5 μm ($p < 0.0001$, see Fig. 9*A*3–*A*7). One-hundred datasets were generated and analyzed. Figure 9*A*8 is the cumulative histogram of p values calculated for the 100 datasets. Among these 100 sets, 35 had p values lower than 0.01. Therefore, under the periodic distribution described above, the analysis reported $p < 0.01$ in 35% of cases.

The same analysis was performed for different strengths of periodicity by changing the probability at the troughs of the sinusoid. When the probability at the trough was 1/4 and 1/9, periodicity with $p < 0.01$ was detected in 15% and 49% of cases, respectively. These results suggest that to detect periodicity with $p < 0.01$ in ~30–40% of slices, the probability at the peaks has to be at least several-fold higher than that at the troughs.

Second, to evaluate reliability of the periodicity analysis, the above process was performed on the uniform random distribution. Under the uniform random distribution, i.e., when the probability at the troughs was 1 (see Fig. 9*B*), only one among 100 sets had $p < 0.01$ (see Fig. 9*B*8). Therefore, the periodicity analysis gave practically no false-positive results.

Grouping cells into single repeating units. Periodically arranged EGFP(+) cells in brain slices of *Crym*-BAC-EGFP mice were grouped into repeating units in the following manner. Green circles in Figure 11*D*1 represent EGFP(+) cells in a part of the slice shown in Figure 8*A*2. The orientation of periodicity was set to be horizontal. A cell position histogram (see Fig. 11*D*1, black) was generated along the orientation of periodicity with bins of 1 μm in width. The histogram was bandpass filtered with the wavelength range used in the significance test. In this example, the wavelength range was 27.5–30.5 μm. The filtered curve (see Fig. 11*D*1, red solid line) was plotted along with the cell positions, and the cells were divided into single repeating units using the troughs of the filtered curves as borders (see Fig. 11*D*1, red dotted lines).

To confirm that this grouping method worked effectively, phase histograms were generated. The borders of repeating units were assigned phases of 0° and 360°, and the phases of other positions were given by linear interpolation (e.g., the phase of the centers of repeating units was 180°). Figure 11*D*2 is the phase histogram of EGFP(+) cells in slices shown in Figure 8*A*2 and *B*2, prepared from the same mouse. The histogram had a peak at 180° and troughs at 0° and 360°, indicating that cells were more likely located at the centers of repeating units than at the borders. Therefore, the grouping method effectively divided cells into repeating units.

Calculation of P(c-Fos). P(c-Fos) was calculated as follows. First, an EGFP(+)c-Fos(+) cell was selected as a reference cell (see Fig. 11*F*, left, black dot). The number of EGFP(+)c-Fos(+) cells excluding the reference cell and the number of EGFP(+)c-Fos(−) cells were counted in each repeating units. In the left panel of Figure 11*F*, the repeating unit containing the reference cell has three EGFP(+)c-Fos(+) cells excluding the reference cell and no EGFP(+)c-Fos(−) cells. The left repeating unit has no EGFP(+)c-Fos(+) cells and three EGFP(+)c-Fos(−) cells, and the right repeating unit has one EGFP(+)c-Fos(+) cell and two EGFP(+)c-Fos(−) cells. By merging the data from both sides, the data for the adjacent unit was obtained [one EGFP(+)c-Fos(+) cell and five EGFP(+)c-Fos(−) cells].

The same counting was continued using all EGFP(+)c-Fos(+) cells as references, and the total numbers of EGFP(+)c-Fos(+) and EGFP(+)c-Fos(−) cells were obtained for each repeating unit located at positions relative to repeating units containing reference cells. For example, in the left panel of Figure 11*F*, 18 EGFP(+)c-Fos(+) cells and five EGFP(+)c-Fos(−) cells were found in repeating units containing reference cells, and eight EGFP(+)c-Fos(+) cells and 33 EGFP(+)c-Fos(−) cells were found in repeating units adjacent to repeating units containing reference cells. This process was repeated for all slices that showed significant periodicity, and the total numbers of EGFP(+)c-Fos(+) cells and EGFP(+)c-Fos(−) cells were obtained for repeating units containing reference cells, for repeating units adjacent to that containing reference cells, and for repeating units located further from repeating units containing reference cells. For each of these, P(c-Fos) was calculated using the following formula:

$$P(\text{c-Fos}) = \frac{[\text{Number of EGFP}(+)\text{c-Fos}(+)\text{ cells}]}{[\text{Number of EGFP}(+)\text{c-Fos}(+)\text{ cells}] + [\text{Number of EGFP}(+)\text{c-Fos}(-)\text{ cells}]}. \quad (2)$$

To perform an analysis in the tangential orientation at higher spatial resolution, radial bins were placed at specific positions relative to reference cells (see Fig. 11*H*, left). These bins were oriented perpendicular to the orientation of periodicity, and reference cells were at the centers of the central bins. The width and height of the bins were 10 and 120 μm, respectively. The numbers of EGFP(+)c-Fos(+) and EGFP(+)c-Fos(−) cells were counted using these bins, and data from both the left and right sides were merged symmetrically. P(c-Fos) was calculated using the above formula. Analysis was performed separately for target cells located within repeating units containing reference cells and for target cells outside repeating units containing reference cells. To analyze the correlation in the radial orientation, the central radial bin (width = 10 μm, height = 160 μm) was placed in the same manner as above and divided by borders placed at ±20, ±40, ±60, and ±80 μm measured in the radial orientation from reference cells (see Fig. 11*I*, left). The numbers of cells in bins above and below reference cells were merged symmetrically, and P(c-Fos) was calculated as described above. The analysis in the radial orientation was performed only for target cells located within repeating units containing reference cells.

Statistical significance of correlation in c-Fos expression. To examine the statistical significance of correlation in c-Fos expression, the results of real data were compared with those of surrogate data that had randomized c-Fos expression. $N_g^{(i)}$ and $N_{gc}^{(i)}$ represent the numbers of EGFP(+) and EGFP(+)c-Fos(+) cells, respectively, in layer V of the binocular region of the ith slice of the real data. To generate random surrogate data for the ith slice, $N_g^{(i)}$ EGFP(+) cells were located at the same positions as the real EGFP(+) cells. Among these $N_g^{(i)}$ EGFP(+) cells, $N_{gc}^{(i)}$ cells were randomly selected as surrogate EGFP(+)c-Fos(+) cells. After generating one surrogate for each slice, P(c-Fos) was calculated using the surrogate EGFP(+)c-Fos(+) cells. This process was performed N_{Sur} (=10,000) times, by randomly generating surrogates each time. For each relative position, the highest 1% and the median of P(c-Fos) calculated with N_{Sur} surrogates were determined and shown in the figures as a black solid line and a black dashed line, respectively. The significance was determined for each relative position as $P = N_{\text{Exc}}/N_{\text{Sur}}$, where N_{Exc} is the number of surrogates for which P(c-Fos) was higher than that of real data.

P(c-Fos) under random expression was estimated as follows:

$$P_{\text{Rand}} = \frac{1}{\sum_{i=1}^{S} N_{gc}^{(i)}} \sum_{i=1}^{S} \left(N_{gc}^{(i)} \frac{N_{gc}^{(i)} - 1}{N_g^{(i)} - 1} \right), \quad (3)$$

where S is the number of slices. P_{Rand} was close to the median of P(c-Fos) calculated with surrogate data (see Fig. 11*G–J*, blue and black dashed lines, respectively), indicating that the formula gives an accurate estimation.

Robustness of the P(c-Fos) calculation. The robustness of the correlation analysis was confirmed as follows. First, to confirm that the results of the high-resolution analysis did not depend on the size of bins, the widths of the bins were changed from 10 to 8.5 or 14 μm and the same analysis as shown in Figure 11*H* was performed (see Fig. 11*J*1,2, respectively). This analysis was performed separately for target cells located within or outside repeating units containing reference cells. For target cells within repeating units containing reference cells, correlation in the central bin was significant in analyses with both bin widths (see Fig. 11*J*1,2; ****$p <$ 0.0001, indicated by the thick red lines). When the bin width was 8.5 μm, the correlation in the second bin was also significant ($p = 0.027$), whereas that in the third bin was insignificant ($p > 0.1$). When the bin width was 14 μm, the correlations in the second and third bins were both insignificant ($p > 0.07$). For target cells outside repeating units containing reference cells, no significant correlation was found in these analyses (see Fig. 11*J*1,2, indicated by the thin red lines). Therefore, the results of the correlation analysis did not depend on bin widths.

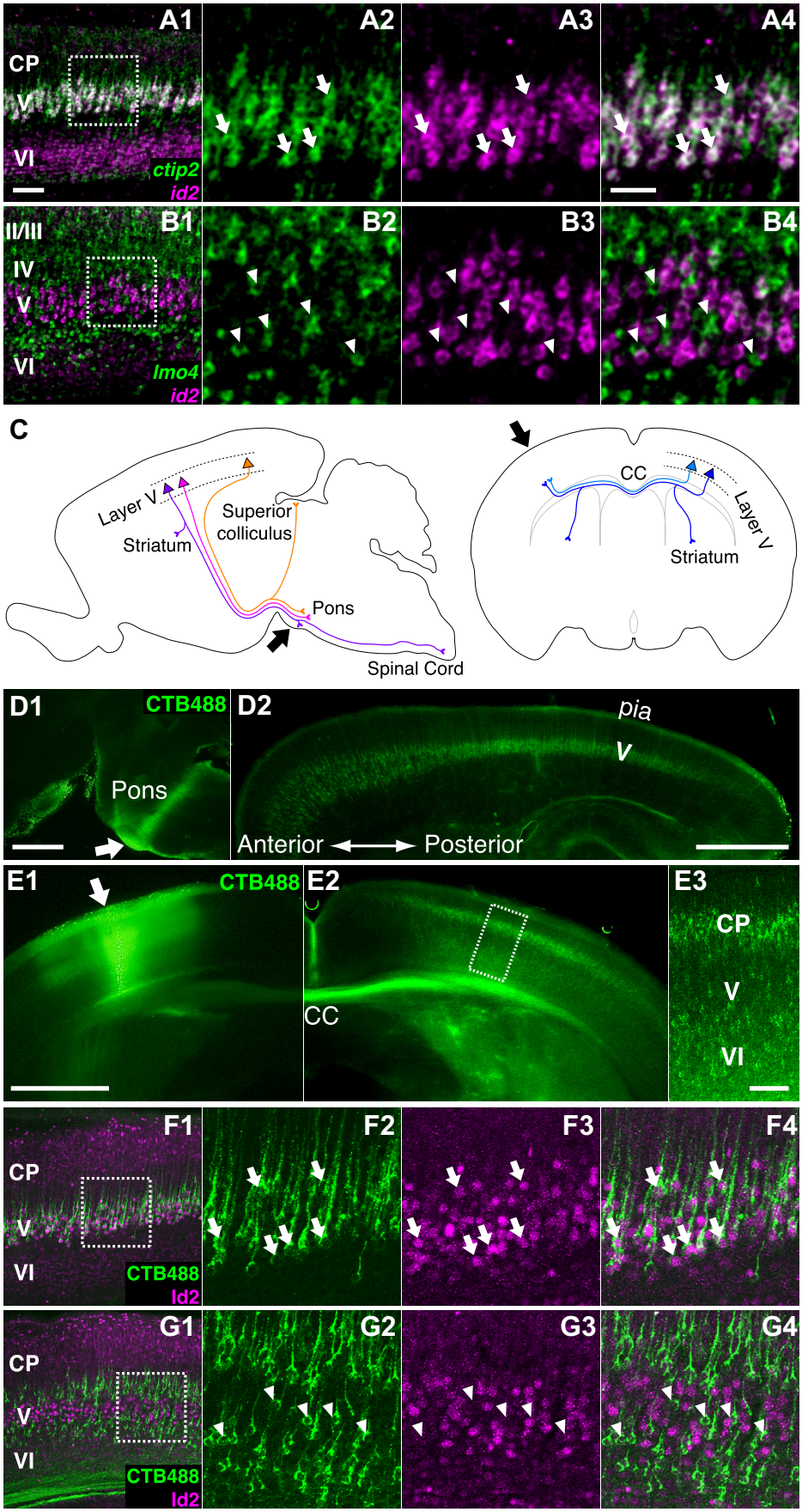

Figure 1. Cell type analysis in the visual cortex in young mice. ***A***, Sagittal slice of the primary visual cortex (V1) at P4 showing *id2* (magenta) and *ctip2* (green) mRNAs labeled by FISH. ***A1***, Low-magnification photograph. ***A2–A4***, High-magnification photograph of the boxed region in ***A1*** showing *ctip2* mRNA (***A2***), *id2* mRNA (***A3***), and both (***A4***). (*Figure legend continues.*)

Second, it was examined whether the result is robust even when the analysis is limited to cells that exhibited relatively strong c-Fos expression. *P*(c-Fos) was calculated using 121 EGFP(+)c-Fos(+) cells that exhibited relatively strong c-Fos expression among the 173 EGFP(+)c-Fos(+) cells used in the original analysis. The analysis was performed using bins of 14 μm in width because the reduction in the number of EGFP(+)c-Fos(+) cells made the result with bins of 10 μm in width noisier. As expected from the smaller number of EGFP(+)c-Fos(+) cells, *P*(c-Fos) was lower than that calculated with the 173 EGFP(+)c-Fos(+) cells (see Fig. 11*J*3). However, for target cells located within repeating units containing reference cells, the correlation at the central bin was significant (see Fig. 11*J*3; $^{****}p < 0.0001$, indicated by the thick red line). In contrast, no significant correlation was found for target cells outside repeating units containing reference cells (see Fig. 11*J*3, indicated by the thin red lines). Therefore, the results of the correlation analysis were robust even when only cells with relatively stronger c-Fos expression were analyzed.

Results

Specific expression of *id2* in subcerebral projection neurons in the early visual cortex

To investigate the cell type that expresses *id2* in layer V of the visual cortex, we first compared mRNA expression of *id2* with that of *ctip2*, which is expressed in subcerebral projection neurons but not in callosal projection neurons (Arlotta et al., 2005; Molnár and Cheung, 2006; Molyneaux et al., 2007). We performed the analysis in the early visual cortex because *id2* expression is strong in young mice. In layer V of the visual cortex of P4 mice (Fig. 1*A*), 97.2% of *id2* mRNA(+) cells were *ctip2* mRNA(+) [3 mice, 7 slices, 953 *id2* mRNA(+) cells, 926 *id2* mRNA(+)*ctip2* mRNA(+) cells, 95% confidence interval (CI) 96.1%–98.0%]. Subsequently, we performed double labeling for mRNAs of *id2* and *lmo4* (LIM domain only 4). In layer V, *lmo4* is excluded from subcerebral projection neurons and expressed by callosal projection neurons (Arlotta et al., 2005; Molnár and Cheung, 2006; Molyneaux et al., 2007) (Fig. 1*B*). We analyzed the P7 brain because the visual cortex exhibited strong *lmo4* mRNA expression at this stage. In layer V, only 3.3% of *id2* mRNA(+) cells were *lmo4* mRNA(+) [2 mice, 5 slices,152 *id2* mRNA(+) cells, 5 *id2* mRNA(+)*lmo4* mRNA(+) cells, 95% CI 1.3%–6.8%]. These data suggest that, in layer V, *id2* mRNA is expressed specifically in subcerebral projection neurons but not in callosal projection neurons.

To further substantiate these results, we retrogradely labeled specific cell types and investigated Id2 protein expression. Tracer injection and perfusion were performed at P2 and P4, respectively. Subcerebral projection neurons were labeled by injecting the retrograde tracer cholera toxin subunit B conjugated with Alexa 488 (CTB488) into the pyramidal tract at the pons-midbrain junction (Fig. 1*C*, left, *D*). After slicing the visual cortex, strongly labeled slices were further stained for Id2 protein expression (Fig. 1*F*). In layer V of the visual cortex, 98.4% of retrogradely labeled subcerebral projection neurons were Id2 protein (+) [2 mice, 4 slices, 184 CTB488(+) cells, 181 CTB488(+)Id2(+) cells, 95% CI 95.9%–99.6%], and 87.2% of Id2 protein(+) cells in layer V were retrogradely labeled subcerebral projection neurons [2 mice, 4 slices, 344 Id2(+) cells, 300 Id2(+)CTB488(+) cells, 95% CI, 83.9%–90.1%]. Therefore, virtually all subcerebral projection neurons express Id2 protein, and the majority of Id2 protein(+) cells in layer V are subcerebral projection neurons. Because retrograde labeling may not label all subcerebral projection neurons, the actual probability that an Id2(+) cell in layer V is a subcerebral projection neuron could be even >87.2%.

In addition, we labeled callosal projection neurons by injecting CTB488 into the contralateral cortex (Fig. 1*C*, right, *E*). In layer V, only 4.7% of retrogradely labeled callosal projection neurons were Id2 protein(+) [Fig. 1*G*; 2 mice, 4 slices, 172 CTB488(+) cells, 8 CTB488(+)Id2(+) cells, 95% CI 2.3%–8.2%], and only 2.0% of Id2 protein(+) cells were retrogradely labeled callosal projection neurons [Fig. 1*G*; 2 mice, 4 slices, 343 Id2(+) cells, 7 Id2(+)CTB488(+) cells, 95% CI 1.0%–3.8%]. Therefore, almost no callosal projection neurons in layer V express Id2.

Together, these data demonstrate that *id2* is a neuronal subtype-specific marker of subcerebral projection neurons in layer V of the young visual cortex. Therefore, we decided to investigate the micro-organization of subcerebral projection neurons.

Periodic organization of subcerebral projection neurons in the early visual cortex

Because the nonrandom distribution of *id2*(+) cells was observed in the posterior visual cortex of young mice (Rubenstein et al., 1999), we first investigated the spatial distribution of subcerebral projection neurons in this area. Figure 2*A* illustrates a coronal slice of the posterior visual cortex of P6 mice stained for *id2* mRNA. Consistent with the previous report, neurons expressing *id2* in layer V often formed radial clusters (Fig. 2*B*). Figure 2*C* illustrates the P6 visual cortex stained for *id2* mRNA by FISH and counterstained for nuclei. Although nuclear staining did not show any apparent pattern (Fig. 2*C*1), FISH revealed radial clustering of *id2*(+) cells in layer V (Fig. 2*C*2). Between the clusters of *id2*(+) cells, nuclei of *id2*(−) cells were visible. Consistent with the previous study, these results suggest that *id2*(+) cells tend to form radial clusters in layer V and that these clusters are surrounded by *id2*(−) cells.

←

(*Figure legend continued.*) Arrows indicate cells expressing both *id2* mRNA and *ctip2* mRNAs. Thickness of the slice was 30 μm. Scale bars: (in ***A1***) ***A1***, ***B1***, ***F1***, and ***G1***, 100 μm; (in ***A4***) other panels in ***A***, ***B***, ***F***, and ***G***, 50 μm. ***B***, Sagittal slice of V1 at P7 showing *id2* (magenta) and *lmo4* (green) mRNAs labeled by FISH. ***B1***, Low-magnification photograph. ***B2–B4***, High-magnification photograph of the boxed region in ***B1*** showing *lmo4* mRNA (***B2***), *id2* mRNA (***B3***), and both (***B4***). Arrowheads indicate cells expressing *lmo4* mRNA but not *id2* mRNA. In layer VI, the signal of *id2* mRNA (magenta in ***B1***) is less prominent compared with that at P4 (magenta in ***A1***). Thickness of the slice was 30 μm. ***C***, Schematic illustration of retrograde labeling of pyramidal neurons in layer V. Left, Three subcerebral projection neuron subtypes, corticotectal neurons (orange), corticospinal motor neurons (purple), and corticopontine neurons (magenta), are shown. Right, Callosal projection neurons. Injection sites for retrograde labeling are shown by arrows. ***D***, Retrograde labeling of subcerebral projection neurons. Sagittal slice of a P4 brain injected with CTB488 into the pons-midbrain junction at P2 showing CTB488 labeling. ***D1***, Arrow indicates the injection site. ***D2***, Retrogradely labeled subcerebral projection neurons. Thickness of the slice was 100 μm. Scale bars, 1000 μm. ***E***, Retrograde labeling of callosal projection neurons. Coronal slice of a P4 brain injected with CTB488 into the contralateral cortex at P2 showing CTB488 labeling. ***E1***, Arrow indicates the injection site. ***E2***, Retrogradely labeled callosal projection neurons. ***E3***, High-magnification photograph of the boxed region in ***E2***. Thickness of the slice was 100 μm. Scale bars: (in ***E1***) ***E1***, ***E2***, 1000 μm; in ***E3***, 100 μm. ***F***, Coronal slice of V1 at P4 showing Id2 protein (magenta) labeled by immunohistochemistry (IHC) and subcerebral projection neurons (green) retrogradely labeled by injecting CTB488 into the pons-midbrain junction at P2. ***F1***, Low-magnification photograph. ***F2–F4***, High-magnification photograph of the boxed region in ***F1*** showing CTP488 labeling (***F2***), Id2 protein (***F3***), and both (***F4***). Arrows indicate subcerebral projection neurons expressing Id2 protein. In layer VI, the signal of Id2 protein (magenta in ***F1***) is less prominent compared with that of *id2* mRNA at P4 (magenta in ***A1***). Thickness of the slice was 100 μm. ***G***, Coronal slice of V1 at P4 showing Id2 protein (magenta) labeled by IHC and callosal projection neurons (green) retrogradely labeled by injecting CTB488 into the contralateral cortex at P2. ***G1***, Low-magnification photograph. ***G2–G4***, High-magnification photograph of the boxed region in ***G1*** showing CTP488 labeling (***G2***), Id2 protein (***G3***), and both (***G4***). Arrowheads indicate callosal projection neurons without Id2 protein expression. In layer VI, the signal of Id2 protein (magenta in ***G1***) is less prominent compared with that of *id2* mRNA at P4 (magenta in ***A1***). Thickness of the slice was 100 μm. CC, Corpus callosum; CP, cortical plate; Cortical layers are shown.

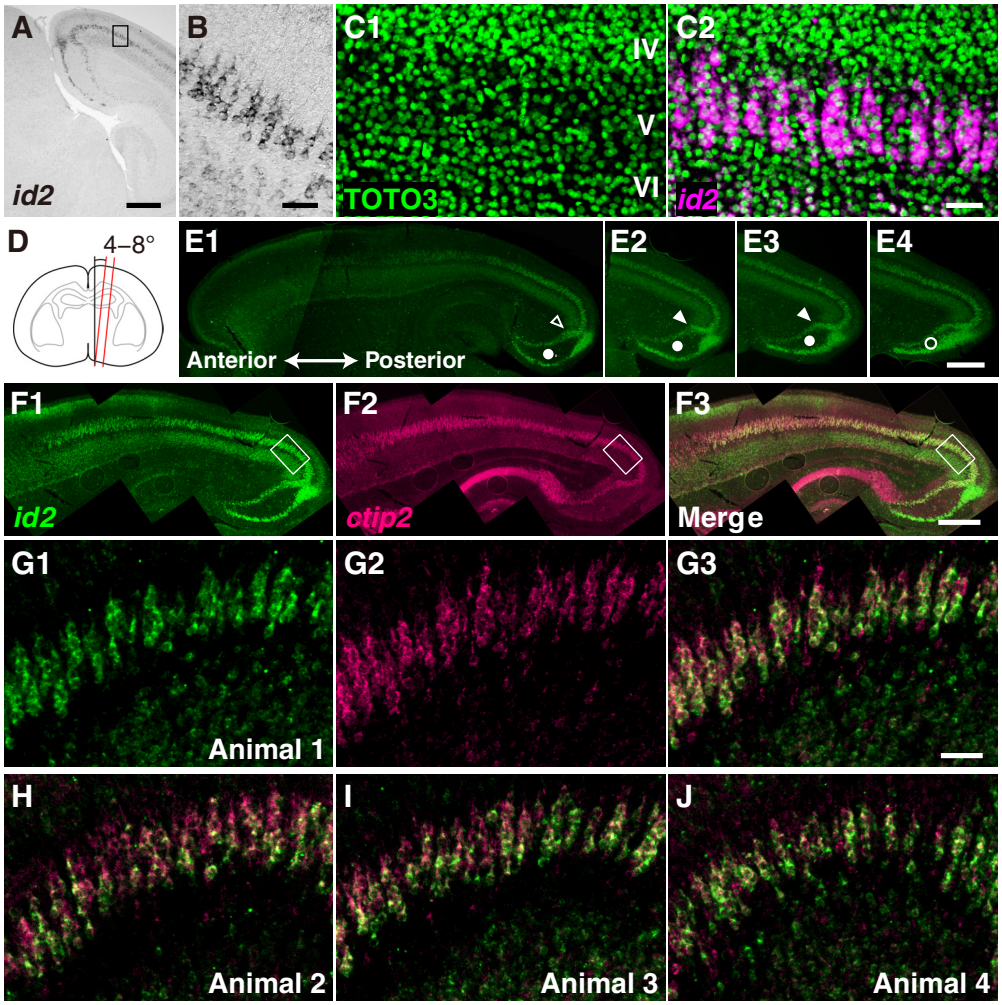

Figure 2. Periodic arrangement of *id2*(+) cells in the visual cortex of young mice. ***A***, ***B***, Coronal slices of the posterior visual cortex at P6 stained for *id2* mRNA with NBT/BCIP. ***A***, Low-magnification photograph. Strong expression in layer V and weak expression in layer II/III and VI are visible. Scale bar, 500 μm. ***B***, High-magnification photograph of the area indicated by a rectangle in ***A*** showing radial clusters of *id2*(+) cells in layer V. Scale bar, 50 μm. ***C***, Coronal slice of the visual cortex at P6 stained for *id2* mRNA (magenta) by FISH and for nuclei (green) by TOTO3 staining. Layers are indicated in ***C1***. Scale bar: (in ***C2***) ***C1***, ***C2***, 50 μm. ***D***, Schematic illustration of parasagittal slicing. The slicing plane (red) was tilted by 4–8° from the median plane (black). ***E***, Preparation of parasagittal slices. P4 brains were sliced into the orientation shown in ***D*** (30 μm thickness) and stained for *id2* mRNA by FISH. Slices in ***E1*** to ***E4*** are in the lateral-to-medial order. Arrowheads and circles denote features used for selecting slices (see Materials and Methods). Scale bar: (in ***E4***) ***E1–E4***, 500 μm. ***F***, Low-magnification photographs of parasagittal slices of a P4 mouse stained using FISH for *id2* mRNA (green, ***F1*** and ***F3***) and *ctip2* mRNA (purple, ***F2*** and ***F3***). Scale bar: (in ***F3***) ***F1–F3***, 500 μm. ***G***, High-magnification photograph of the posterior visual cortex indicated by rectangles in ***F***. Scale bar: (in ***G3***) ***G–J***, 50 μm. ***H–J***, Posterior visual cortices of three other P4 mice visualized similarly to ***G3***.

These clusters were often located approximately periodically in the tangential orientation. In Figure 2*C*2, ~13 radial clusters are visible, and they are located approximately periodically in the tangential orientation. The wavelength of periodicity, i.e., the distance between radial axes of adjacent clusters, was ~25 μm. To further characterize the possible periodic arrangement, we analyzed parasagittal slices because their cutting angle can be precisely controlled by measuring the angle relative to the median plane. Because clusters in coronal slices appeared tilted relative to the median plane (Fig. 2*B*), we tilted the cutting angle by 4–8° from the median plane (Fig. 2*D*; Materials and Methods). The thickness of the slices was 30 μm, which is similar to the wavelength of observed periodicity. We analyzed a posterior region in the visual cortex (Fig. 2*E*,*F*; Materials and Methods).

We stained slices for *id2* and *ctip2* mRNA to visualize subcerebral projection neurons (Fig. 2*F*,*G*). Similar to coronal slices, we often observed radial clusters of *id2*(+) cells in layer V (Fig. 2*G*1). The distance between the radial axes of two adjacent clusters was ~23 μm, similar to that in coronal slices. This distance was approximately similar for all pairs of adjacent clusters (Fig. 2*G*1), suggesting a periodic arrangement. A similar periodic arrangement was visible in the photograph showing *ctip2* mRNA (Fig. 2*G*2), in agreement with its coexpression with *id2* in subcerebral projection neurons (see above). Radial clustering and periodic arrangement were similarly found across different individual mice (Fig. 2*H–J*). Orientation and size of clusters were similar among these individuals (Fig. 2*G–J*).

We performed statistical analysis of periodicity. Figure 3 illustrates the analysis of the slice shown in Figure 2*H*. The positions of *id2*(+) cells were measured relative to the center line of layer V (Fig. 3*A*1,2) because layer V was curved. Using these positions, we generated a histogram of relative positions that illustrates the frequency of finding an *id2*(+) cell at a position relative to another *id2*(+) cell (Fig. 3*A*3,4). As illustrated in Figure 3*A*4, the histogram had parallel stripes. These parallel stripes suggest periodicity because they indicate that when an *id2*(+) cell is found,

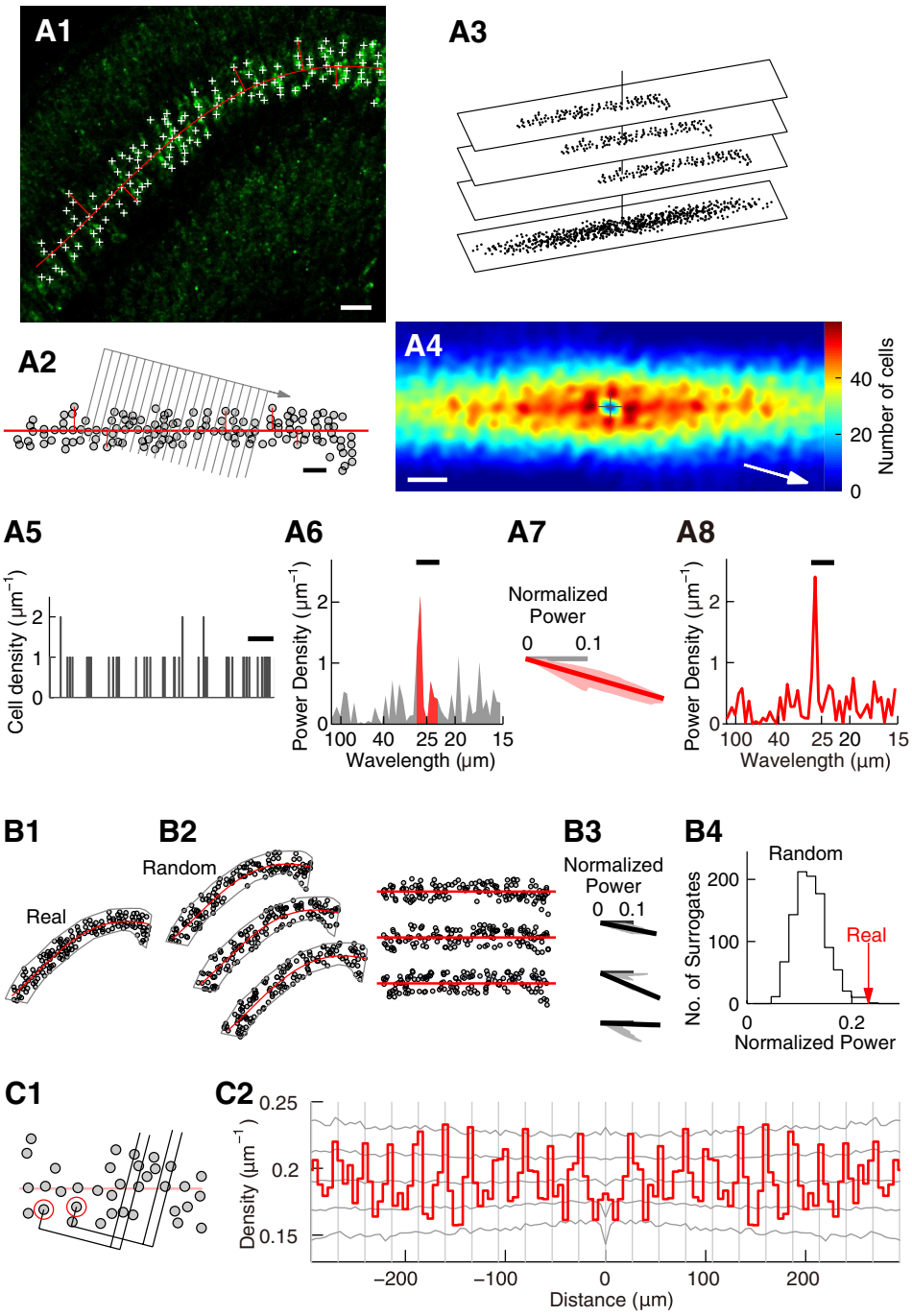

Figure 3. Statistical analysis of periodicity. ***A–C***, Statistical analysis of periodicity performed on the slice shown in Figure 2*H*. ***A***, Histogram of relative positions and power spectrum. ***A1***, The same slice as in Figure 2*H* showing *id2* mRNA expression (green). *id2*(+) cells in layer V are labeled with plus signs. The center line of layer V is indicated by a curved red line. Short straight red lines are lines used to measure the positions of *id2*(+) cells relative to the center line of layer V (see Materials and Methods). Scale bar, 50 μm. ***A2***, Gray circles denote the positions of *id2*(+) cells in layer V measured relative to the center line of layer V. The center line of layer V is shown as a horizontal red line. The short lines used to measure the positions of *id2*(+) cells are also shown. Gray parallel lines denote the borders of bins used to make the cell position histogram. Gray arrow indicates the orientation of the alignment of bins. In this example, the orientation is approximately perpendicular to the stripes in ***A4***. Scale bar, 50 μm. ***A3***, Method to construct the histogram of relative positions (see Materials and Methods). ***A4***, Histogram of relative positions generated for the positions of the *id2*(+) cells shown in ***A2***, smoothed with the Gaussian function ($\sigma = 5.5$ μm). Origin is shown by the plus sign and the number of cells is shown in color. Scale bar, 50 μm. ***A5***, Cell position histogram of the positions of the *id2*(+) cells shown in ***A2*** generated with the bins shown in ***A2***. The bin width was 1 μm. Scale bar, 30 μm. ***A6***, Power spectrum of the histogram in ***A5***. Bar indicates the wavelength range used for analysis (22.5–27.5 μm). The area under the bar is shown in red. ***A7***, Red, Normalized power of the wavelength range of 22.5–27.5 μm measured by rotating the bins. The orientation of periodicity is shown by the thick line. Gray, Horizontal axis. ***A8***, Power spectrum of cell distribution, prepared for the orientation of periodicity. Bar indicates the wavelength range used for analysis (22.5–27.5 μm). ***B***, Generation and analysis of random surrogates to estimate statistical significance of periodicity. ***B1***, Distribution of *id2*(+) cells in layer V shown in ***A1***. Gray line denotes the area to be analyzed. Red line depicts the center line of layer V. ***B2***, Left, Three examples of random surrogates. Right, The positions of surrogate cells measured relative to the center line of layer V. ***B3***, Normalized power measured as that in ***A7***. The orientation of periodicity is indicated by a thick line. ***B4***, Significance test. The red arrow ("Real") indicates the normalized power measured for the real data in the orientation of periodicity. The gray line ("Random") is the histogram of the normalized power measured for 1000 surrogate datasets with random cell distribution. Note that almost all surrogates had normalized power smaller than that of the real data. The significance $p = 0.001$. ***C***, Autocorrelation analysis. ***C1***, Construction of the autocorrelogram (see Materials and Methods). ***C2***, Autocorrelogram of cell positions shown in ***A2***, prepared for the orientation of periodicity. Gray vertical lines are placed every 26.7 μm. Gray lines drawn sideways show the highest 2.5%, the highest 15.9%, the median, the lowest 15.9%, and the lowest 2.5% of autocorrelograms calculated for the 1000 surrogates.

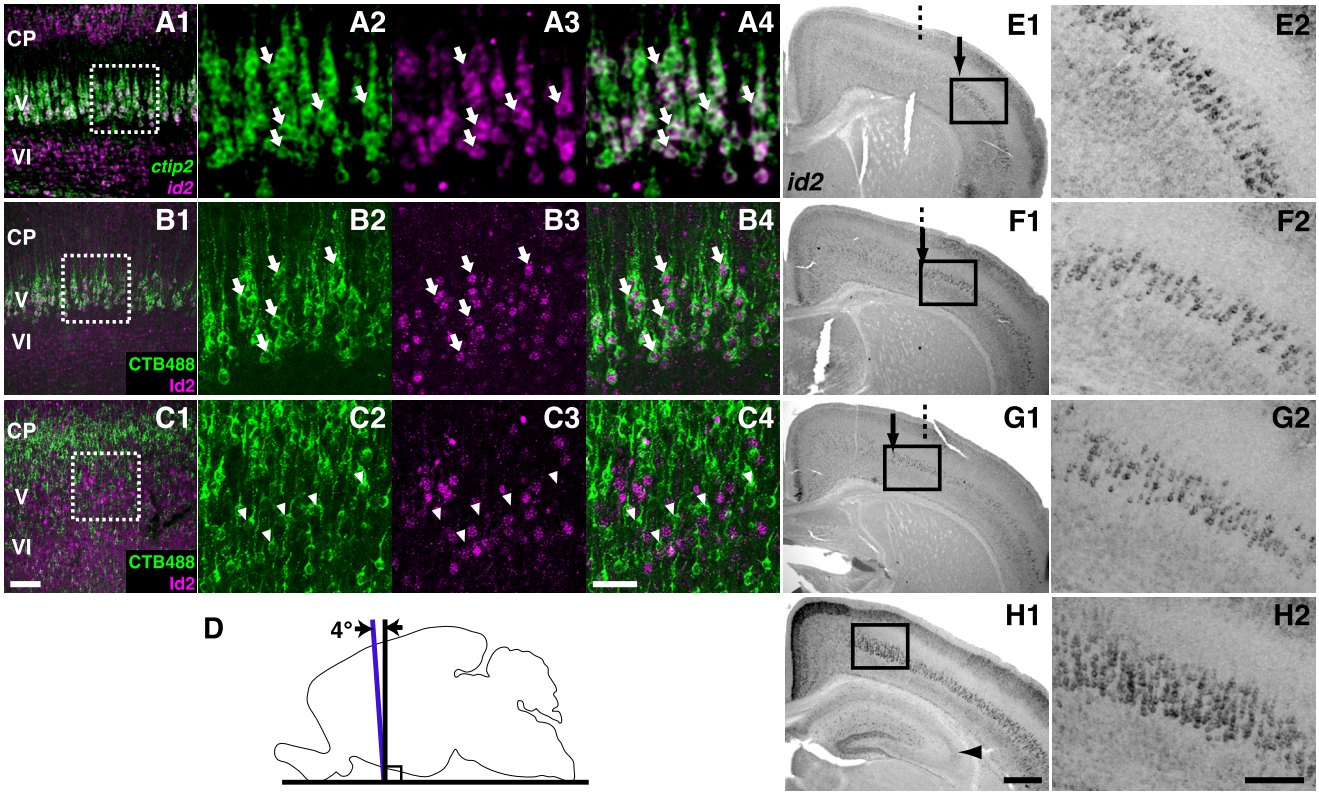

Figure 4. Cell type analysis and slicing of the somatosensory cortex. ***A–C,*** Specific expression of *id2* in subcerebral projection neurons in the primary somatosensory cortex (S1). CP, Cortical plate; V and VI, layers V and VI, respectively. ***A***, Sagittal slice of the S1 at P4 showing *id2* (magenta) and *ctip2* (green) mRNAs labeled by FISH. ***A1***, Low-magnification photograph. ***A2–A4***, High-magnification photographs of the boxed region in ***A1*** showing *ctip2* mRNA (***A2***), *id2* mRNA (***A3***), and both (***A4***). Arrows indicate cells expressing both *id2* mRNA and *ctip2* mRNA. Thickness of the slice was 30 μm. ***B***, Coronal slice of S1 at P4 showing Id2 protein (magenta) labeled by immunohistochemistry (IHC) and subcerebral projection neurons (green) retrogradely labeled with CTB488 injected into the pons-midbrain junction at P2. ***B1***, Low-magnification photograph. ***B2–B4***, High-magnification photograph of the boxed region in ***B1*** showing CTP488 labeling (***B2***), Id2 protein (***B3***), and both (***B4***). Arrows indicate subcerebral projection neurons expressing Id2 protein. Thickness of the slice was 100 μm. ***C***, Coronal slice of S1 at P4 showing Id2 protein (magenta) labeled by IHC and callosal projection neurons (green) retrogradely labeled with CTB488 injected into the contralateral cortex at P2. ***C1***, Low-magnification photograph. ***C2–C4***, High-magnification photographs of the boxed region in ***C1*** showing CTP488 (***C2***), Id2 protein (***C3***), and both (***C4***). Arrowheads indicate callosal projection neurons without Id2 protein expression. Thickness of the slice was 100 μm. Scale bars: (in ***C1***) ***A1***, ***B1***, and ***C1***, 100 μm; (in ***C4***) for other panels, 50 μm. ***D***, Schematic illustration of slicing. Brains were sliced in the orientation shown by the purple line to analyze periodic organization in the somatosensory cortex. Black vertical line denotes the coronal plane. ***E–H***, Slices prepared as in ***D*** from a single mouse, stained for *id2* mRNA with NBT/BCIP and shown in the anterior-to-posterior order. ***E1***, ***F1***, ***G1***, and ***H1*** are low-magnification photographs. Arrows indicate positions from which strong *id2* mRNA expression in layer V extended laterally. Dotted lines are the center between the median plane and the lateral edge of the brain. Arrowhead in ***H1*** denotes the hippocampus. ***E2***, ***F2***, ***G2***, and ***H2*** are high-magnification photographs of the boxed regions in the low-magnification photographs. Scale bars: (in ***H1***) ***E1***, ***F1***, ***G1***, and ***H1***, 600 μm; (in ***H2***) ***E2***, ***F2***, ***G2***, and ***H2***, 200 μm. The slices shown in ***F*** and ***G*** are also shown in Figure 5*A* and *B*, respectively.

other *id2*(+) cells tend to be located immediately above or below it in a tilted direction or in tilted columnar areas tangentially shifted in a periodic manner.

We quantified periodicity by calculating the power spectrum of cell distribution and investigated the statistical significance by comparing the results to those expected under the random distribution (Fig. 3*A*,*B*; Materials and Methods). Statistically significant periodicity was detected ($p = 0.001$, wavelength range = 22.5–27.5 μm; Fig. 3*B*4) in an orientation (the orientation of periodicity; Fig. 3*A*4, arrow) slightly rotated from the center line of layer V. We confirmed that this method gives practically no false positives (Materials and Methods). Consistent with this periodicity, the power spectrum prepared for the orientation of periodicity had a sharp peak, and the peak wavelength was 26.5 μm (Fig. 3*A*8). The autocorrelogram, which represents the average number of *id2*(+) cells found in a position relative to another *id2*(+) cell, showed oscillation up to 10 cycles when measured in the orientation of periodicity (Fig. 3*C*1,2). Therefore, the periodic arrangement continues for at least several cycles without significant shifts in wavelength or phase.

Among 24 slices prepared from four mice, 15 slices showed significant periodicity ($p < 0.01$ for either of the two wavelength ranges of 20–25 μm and 22.5–27.5 μm). The total significance (P_{Total}) was $<1 \times 10^{-19}$, and the peak wavelength was 23.2 ± 2.4 μm (mean ± SD). These results indicate that the distribution of subcerebral projection neurons in the visual cortex of young mice is not random but significantly periodic. Part of the reason for not detecting periodicity in all slices may be the limited sensitivity of our method (see Materials and Methods).

Specific expression of *id2* in subcerebral projection neurons in the somatosensory cortex

To investigate whether the periodic organization existed in other cortical areas, we examined the somatosensory cortex. For this purpose we examined whether *id2* is specifically expressed in subcerebral projection neurons in layer V of the somatosensory cortex. Analysis of mRNA expression in layer V of the somatosensory cortex of P4 mice revealed that 98.0% of *id2* mRNA(+) cells were *ctip2* mRNA(+) [Fig. 4*A*; 3 mice, 7 slices, 1070 *id2* mRNA(+) cells, 1049 *id2* mRNA(+)*ctip2* mRNA(+) cells, 95% CI 97.2%–98.7%]. We did not perform double labeling of *id2* and

lmo4 because *lmo4* mRNA expression was too weak in the somatosensory cortex.

When subcerebral projection neurons were retrogradely labeled with CTB488 (Fig. 4*B*), 97.3% of retrogradely labeled cells in layer V were Id2 protein(+) [2 mice at P4, 4 slices, 187 CTB488(+) cells, 182 CTB488(+)Id2(+) cells, 95% CI 94.5%–98.9%], and 92.5% of Id2 protein(+) cells in layer V were retrogradely labeled [3 mice, 5 slices, 345 Id2(+) cells, 319 Id2(+)CTB488(+) cells, 95% CI 89.7%–94.7%]. In contrast, when callosal projection neurons were retrogradely labeled (Fig. 4*C*), only 1.2% of retrogradely labeled cells in layer V were Id2 protein(+) [2 mice, 4 slices, 174 CTB488(+) cells, 2 CTB488(+)Id2(+) cells, 95% CI 0.2%–4.2%], and only 0.9% of Id2 protein(+) cells in layer V were retrogradely labeled [3 mice, 5 slices, 337 Id2(+) cells, 3 Id2(+)CTB488(+) cells, 95% CI 0.6%–3.1%].

Together, similarly to the visual cortex, *id2* was expressed specifically in subcerebral projection neurons in layer V of the somatosensory cortex.

Periodic organization in the somatosensory cortex

We performed periodicity analysis on the somatosensory cortex at P9, because *id2* expression in the somatosensory cortex was sufficiently strong until this age. In Figure 4*E–H*, brain slices prepared as described in Materials and Methods are aligned in the anterior-to-posterior order. We investigated the most medial positions that showed strong *id2* expression in each slice (Fig. 4*E2–H2*). In these areas, *id2*(+) cells in layer V were sparser than those in the P4 visual cortex. However, they tended to align radially to form stripes, and these stripes were located approximately periodically (Fig. 4*E2–H2*). The orientation of periodicity gradually changed depending on the medial–lateral position of the investigated area (Fig. 4*E2–H2*).

We performed statistical analyses on slices made from specific anterior–posterior positions in the brain corresponding to Figure 4*F* and *G* (Materials and Methods). Because layer V in the analyzed area was not strongly curved, we performed the periodicity analysis using the raw coordinates of cell positions. For example, for the slice shown in Figs. 4*F* and 5*A*, the histogram of relative positions showed a periodically striped pattern (Fig. 5*A3*), and significant periodicity was detected ($p = 0.0028$, wavelength range = 30–35 μm). The power spectrum of cell distribution prepared for the orientation of periodicity had a sharp peak (Fig. 5*A4*; peak wavelength = 33.3 μm). The autocorrelogram showed oscillation up to 600 μm or 16 cycles (Fig. 5*D*), indicating that the periodic arrangement continued for several hundred micrometers without significant shifts in wavelength or phase.

Similar periodicity was detected in other slices from the same mouse or those from different individual mice. Figure 5*B* shows another slice from the same mouse as shown in Figure 5*A*, and Figure 5*C* shows a slice from another mouse. These slices exhibited significant periodicity ($p = 0.0022$, wavelength range = 30–35 μm and $p = 0.0011$, wavelength range = 32.5–37.5 μm, respectively), and the peak wavelengths were 32.1 and 36.7 μm, respectively (Fig. 5*B4*,*C4*). Among 23 slices from two mice, 12 exhibited significant periodicity ($p < 0.01$ for either of the two wavelength ranges, 30–35 μm and 32.5–37.5 μm), resulting in $P_{\mathrm{Total}} < 1 \times 10^{-14}$, and the peak wavelength was 33.4 ± 2.1 μm (mean ± SD). Therefore, the distribution of *id2*(+) cells in layer V of the somatosensory cortex had significant periodicity with a longer wavelength than that in the early visual cortex.

Nonclonal origin of neurons in single repeating units

The above results revealed the periodic arrangement of *id2*(+) cells. It is possible that this arrangement is a remnant of radial cortical development. In cortical development, pyramidal cells originate on the ventricular side and migrate mostly in the radial direction (Hatten, 1999). Therefore, neurons originating from a single cortical progenitor cell may align radially to form a single repeating unit. This hypothesis predicts that *id2*(+) cells are closer in lineage to *id2*(+) cells in the same repeating unit than to those in neighboring units.

To examine this hypothesis, we labeled sibling neurons using *Cre-ER*, which encodes the mutant Cre protein (Cre-ER) that is regulated by tamoxifen (Danielian et al., 1998; Hayashi and McMahon, 2002). We generated a mouse strain, brain lipid-binding protein (BLBP) promoter-*Cre-ER* (*BLBP-Cre-ER*; Fig. 6*A*), carrying the *Cre-ER* gene driven by the BLBP promoter, which activates gene expression in cortical progenitor cells (Feng and Heintz, 1995; Anthony et al., 2004). *BLBP-Cre-ER* mice were crossed with the *loxP*-βgeo-stop-*loxP*-EGFP reporter mice (the Z/EG mice) (Novak et al., 2000), and tamoxifen was administered to pregnant females (Fig. 6*A*). In embryos carrying both transgenes, tamoxifen induced Cre-ER to catalyze chromosomal excision in randomly selected cortical progenitor cells, resulting in EGFP expression in their progeny (Fig. 6*A*,*B*). We adjusted the time of tamoxifen administration so that mice had EGFP(+) neuron clusters that included layer V neurons and had most probably originated from single cortical progenitor cells.

Figure 6*C* shows a cluster of five EGFP(+) pyramidal neurons (green) in layer V that were most probably siblings, and thus closer in lineage to each other than to nonlabeled neurons. Of these EGFP(+) neurons, three expressed *id2* mRNA (Fig. 6*C–E*, arrowheads). These EGFP(+)*id2*(+) cells did not align radially, but they were distributed tangentially across ~55 μm in three different radial clusters of *id2*(+) cells (Fig. 6*E*, arrowheads). Because all three of these *id2*(+) clusters contained both EGFP(−) and EGFP(+) neurons (Fig. 6*E*), the result is inconsistent with the above hypothesis in that EGFP(+)*id2*(+) cells were not closer in lineage to other cells in the same *id2*(+) clusters but were closer to EGFP(+)*id2*(+) cells in the neighboring *id2*(+) clusters.

We analyzed all clusters that had at least two EGFP(+)*id2*(+) cells in layer V of the visual and somatosensory cortices. We obtained 10 such clusters, and the total number of EGFP(+)*id2*(+) cells in layer V was 35. Although these cells were located within <165 μm in the tangential orientation in each cluster, they did not align radially. Within ±10 μm in the tangential orientation of each EGFP(+)*id2*(+) cell ($n = 35$), only 0.06 ± 0.24 (mean ± SD) other EGFP(+)*id2*(+) cells were found. In contrast, 3.4 ± 2.1 EGFP(−)*id2*(+) cells were found in the same relative position [mean ± SD, $n = 35$ EGFP(+)*id2*(+) cells]. This result indicates that if an EGFP(+)*id2*(+) cell is found, the majority of *id2*(+) cells that are located immediately above or below it are clonally more distant than at least one *id2*(+) cell located at a more tangentially displaced position [note that all clusters contained at least two EGFP(+)*id2*(+) cells]. Thus, in general, two radially located *id2*(+) neurons are not clonally closer than two tangentially located *id2*(+) neurons. These results suggest that single repeating units are not formed by radial alignment of sibling neurons.

Specific expression of EGFP in subcerebral projection neurons in adult *Crym*-BAC-EGFP mice

To investigate whether the periodic organization existed in the adult brain, we labeled subcerebral projection neurons in the

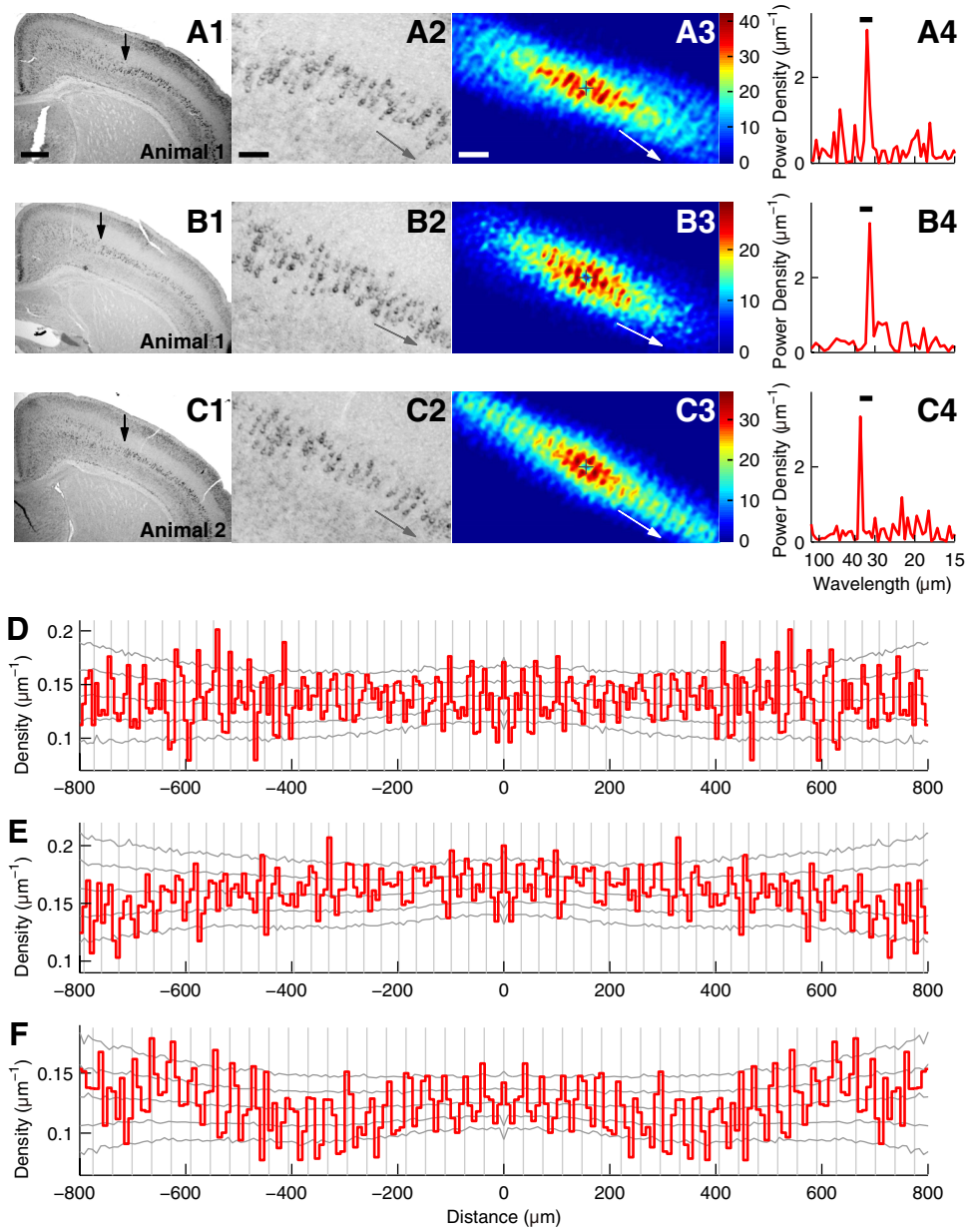

Figure 5. Periodic arrangement of *id2*(+) cells in the somatosensory cortex. ***A***, Analysis of a slice of the P9 somatosensory cortex stained for *id2* mRNA with NBT/BCIP. ***A1***, Low-magnification photograph. Arrow indicates the position from which strong *id2* expression in layer V extended laterally. Approximately 1.1 mm layer V extending laterally from this arrow was used for periodicity analysis. Scale bar: (in ***A1***) ***A1***, ***B1***, and ***C1***, 500 μm. ***A2***, High-magnification photograph of ***A1***. Left edge is approximately at the same position as shown by the arrow in ***A1***. Gray arrow denotes the orientation of periodicity. Scale bar: (in ***A2***) ***A2***, ***B2***, and ***C2***, 100 μm. ***A3***, Histogram of relative positions smoothed with the Gaussian function ($\sigma = 7$ μm). The origin is shown by the plus sign and the number of cells is shown in color. White arrow denotes the orientation of periodicity. Scale bar: (in ***A3***) ***A3***, ***B3***, and ***C3***, 100 μm. ***A4***, Power spectrum of the cell position histogram prepared for the orientation of periodicity. The peak wavelength = 33.3 μm. The bar indicates the wavelength range used for the significance test (30.0 –35.0 μm). $p = 0.0028$. ***B***, Analysis of another slice from the same mouse as used in ***A***. $\sigma = 7$ μm in ***B3***. The peak wavelength in ***B4*** = 32.1 μm. The wavelength range in ***B4*** is 30.0 –35.0 μm. $p = 0.0022$. ***C***, Analysis of a slice from another mouse. $\sigma =$ 7 μm in ***C3***. The peak wavelength in ***C4*** = 36.7 μm. The wavelength range in ***C4*** is 32.5–37.5 μm. $p = 0.0011$. ***D–F,*** Autocorrelograms of cell positions in ***A–C***, respectively. Autocorrelograms were prepared for the orientation of periodicity. Gray vertical lines are placed every 32.2, 33.0, and 36.9 μm, respectively. Gray lateral lines show the highest 2.5%, the highest 15.9%, the median, the lowest 15.9%, and the lowest 2.5% of autocorrelograms calculated for random surrogates.

adult brain. *id2* cannot be used for this purpose, because its expression in layer V becomes weak at ~P14. We therefore investigated whether transgenic mice could be used for labeling. *crym*, a mouse homolog of a human gene encoding ketimine reductase (Hallen et al., 2011), is expressed in a subset of subcerebral projection neurons (Arlotta et al., 2005). Consistently, in layer V of P4 and P9 visual cortices, 100% of *crym* mRNA(+) cells were also *id2* mRNA(+) (Fig. 7*A*; P4, 2 mice, 2 slices, 89 cells, 95% CI 96.7%–100%; P9, 2 mice, 2 slices, 120 cells, 95% CI 97.5%–100%).

Therefore, we investigated *Crym* bacterial artificial chromosome-EGFP (*Crym*-BAC-EGFP) mice, which are transgenic mice carrying a bacterial artificial chromosome (BAC) construct that has *EGFP* inserted in the *crym* locus. We first examined whether EGFP is expressed in *crym*(+) cells in *Crym*-BAC-EGFP mice. In layer V of the visual cortex of P4 *Crym*-BAC-EGFP mice, 82.9% of EGFP(+) cells were *crym* mRNA(+) [Fig. 7*B*; 2 mice, 4 slices, 286 EGFP(+) cells, 237 EGFP(+)*crym* mRNA(+) cells, 95% CI 78.8%–86.4%], indicating that the majority of EGFP(+) cells in layer V were *crym*(+).

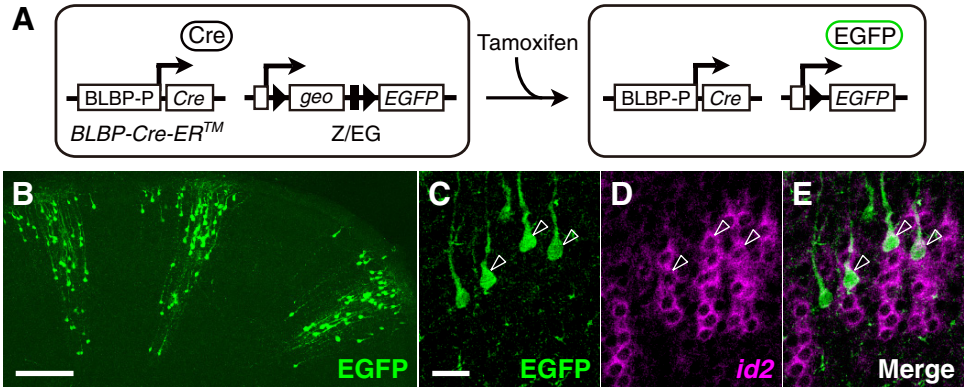

Figure 6. Clonal analysis of *id2*(+) cells. ***A***, Schematic illustration of EGFP induction by chromosomal excision in *BLBP-Cre-ER*; Z/EG embryos. A cortical progenitor cell before tamoxifen administration (left) and after chromosomal excision (right). The BLBP promoter (BLBP-P), *Cre-ER* (*Cre*) and its protein product, the pCAGGS promoter (open rectangle), the *loxP* sequence (triangle), *βgeo* (*lacZ*/neomycin-resistance), the SV40 polyadenylation sequence (solid rectangle), and *EGFP* and its protein product are shown. ***B***, Three clusters of EGFP(+) cells observed in the transgenic mice administered with tamoxifen. The visual cortex of a P4 mouse. Scale bar, 200 μm. ***C–E***, EGFP (***C***) and *id2* mRNA expression (***D***) in the transgenic mice administered with tamoxifen. ***E***, Merged image of ***C*** and ***D***. Arrowheads indicate EGFP(+)*id2*(+) cells. The somatosensory cortex of a P4 mouse. Scale bar: (in ***C***) ***C***, ***D***, and ***E***, 30 μm.

We investigated the cell type of EGFP(+) cells in the adult visual cortex. When subcerebral projection neurons were retrogradely labeled with the retrograde tracer CTB conjugated with Alexa 594 (CTB594), 93.5% of EGFP(+) cells in layer V of the visual cortex were retrogradely labeled [Fig. 7*C*; 2 mice, P23 and P50, 4 slices, 340 EGFP(+) cells, 318 EGFP(+)CTB594(+) cells, 95% CI 90.9%–95.6%], and 79.9% of retrogradely labeled cells in layer V were EGFP(+) [2 mice, P23 and P50, 4 slices, 338 CTB594(+) cells, 270 EGFP(+)CTB488(+) cells, 95% CI 76.0%–83.4%]. In contrast, when callosal projection neurons were retrogradely labeled, none of the retrogradely labeled cells in layer V were EGFP(+) [Fig. 7*D*; 2 mice, P30 and P78, 4 slices, 326 CTB594(+) cells, 0 CTB594(+)EGFP(+)cells, 95% CI 0%–0.9%], and none of the EGFP(+) cells in layer V were retrogradely labeled [2 mice, P30 and P78, 4 slices, 340 EGFP(+) cells, 0 EGFP(+)CTB594(+) cells, 95% CI 0%–0.9%]. Therefore, in layer V of the visual cortices in *Crym*-BAC-EGFP mice, EGFP was expressed specifically in subcerebral projection neurons but not in callosal projection neurons.

Periodic organization in the adult visual cortex

We examined whether EGFP-labeled subcerebral projection neurons in the adult *Crym*-BAC-EGFP mice were periodically arranged. For this purpose, we investigated the adult visual cortex including the binocular region. Brain slices containing the binocular region were prepared as described in the Materials and Methods (Fig. 7*E–H*). Because layer V in the analyzed area was nearly straight, the analysis was performed with raw coordinates of cell positions. Figure 8*A* shows a slice of this area prepared from a P41 mouse. In layer V, EGFP(+) cells were sparser than *id2*(+) cells in layer V of the P4 visual or P9 somatosensory cortex and did not generally align contiguously in the radial orientation (Fig. 8*A*2). Under such sparse distribution, periodicity could be not apparent even if the cell arrangement was strongly periodic, as predicated by our simulation (Fig. 9*A*; Materials and Methods). Consistently, periodicity of EGFP(+) cells was generally not apparent (Fig. 8*A*2). However, the statistical analysis revealed strong periodicity. The histogram of relative positions showed a periodically striped pattern (Fig. 8*A*3), and significant periodicity was detected ($p < 0.0001$, wavelength range = 27.5–30.5 μm). The power spectrum of cell distribution prepared for the orientation of periodicity had a sharp peak (the peak wavelength = 28.2 μm).

Similar periodicity was observed in other slices from the same mouse or those from different mice. Figure 8*B* illustrates another slice from the same mouse shown in Figure 8*A*, and Figure 8*C* illustrates a slice prepared from another mouse at P35. These slices exhibited significant periodicity ($p = 0.0007$ and 0.0026, respectively; wavelength range = 27.5–30.5 μm), with the peak wavelengths similar to that for the slice in Figure 8*A* (29.8 and 29.0 μm, respectively; Fig. 8*B*4,*C*4). Autocorrelograms showed strong oscillation (Fig. 8*D–H*), which often continued up to 600 μm (~19 cycles; Fig. 8*H*) or even 900 μm (~31 cycles, Fig. 8*G*), suggesting that the periodic arrangement extended over several tens of cycles.

Among 40 slices prepared from 11 mice, 16 slices from nine mice exhibited significant periodicity [for seven mice, 13 of 25 slices had $p < 0.01$ for the wavelength range 27.5–30.5 μm and the peak wavelength was 28.6 ± 0.6 μm (mean ± SD); for two mice, three of eight slices had $p < 0.01$ for the wavelength range 33.0–37.0 μm, and the peak wavelength was 36.0 ± 2.3 μm (mean ± SD)].Together, the peak wavelength was 30.0 ± 3.1 μm (mean ± SD, 16 slices), and the statistical significance P_{Total} was $<1 \times 10^{-16}$. This result is in agreement with strong periodicity, because simulation indicated that under the sparse distribution, detection of significant periodicity in 40% (16/40) of slices suggested that cell densities at the centers of repeating units are at least several-fold higher than those at the borders (Fig. 9; Materials and Methods).

Therefore, although subcerebral projection neurons labeled with EGFP in *Crym*-BAC-EGFP mice were sparse and tended not to align contiguously in the radial orientation, their distribution in the tangential orientation had significant periodicity.

No periodicity under incorporation of all cell types

We investigated whether the periodic arrangement was observed when all cell types in layer V were incorporated. When we visualized all nuclei, we observed neither columnar nor periodic arrangement (Fig. 2*C*1). In the adult visual cortex of *Crym*-BAC-EGFP mice, even when EGFP(+) subcerebral projection neurons exhibited periodicity (Fig. 10*A*,*B*, green; *C*, red line), no periodicity was detected when all cells in layer V were incorporated (Fig. 10*A*4, green and gray; *C*, black line). Furthermore, when the same number of cells as the real EGFP(+) cells were randomly selected among all layer V cells (Fig. 10*D*), periodicity similar to that observed for the real EGFP(+) cells was detected only in 0.16% of cases (16 of 10,000;

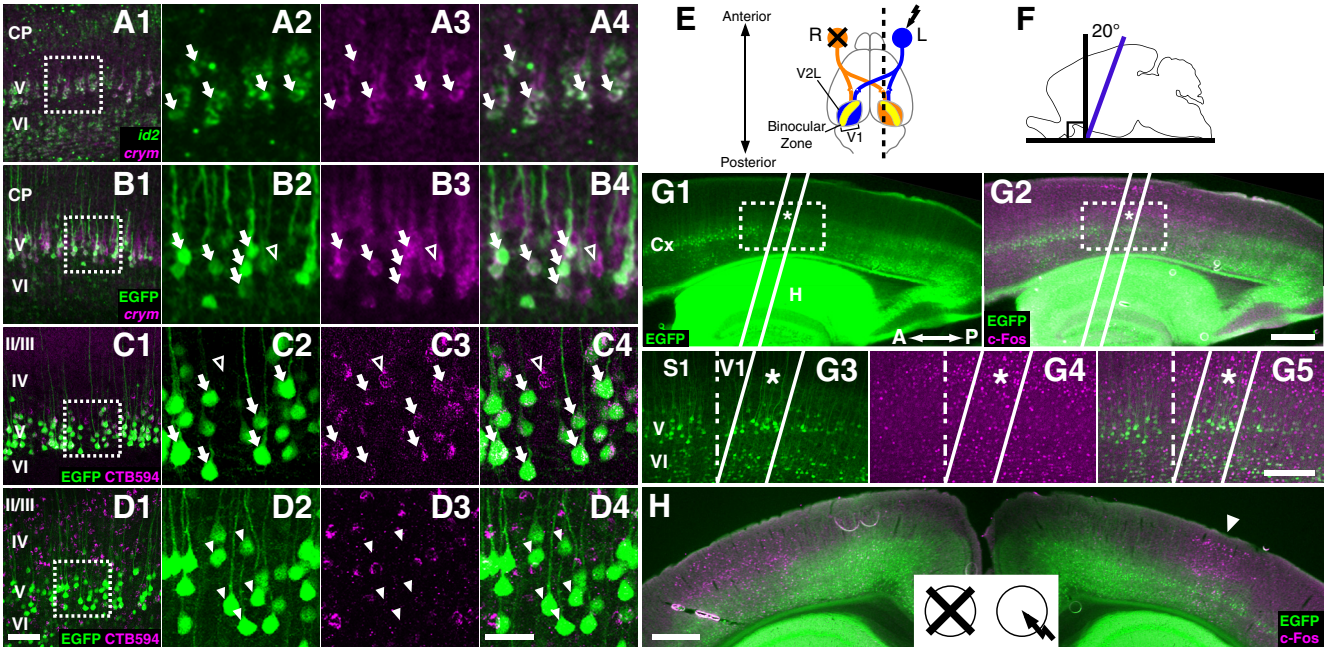

Figure 7. Cell type analysis and slicing of the *Crym*-BAC-EGFP mice. ***A–D***, EGFP in *Crym*-BAC-EGFP mice is a marker for subcerebral projection neurons in the visual cortex of the adult mouse. Cortical layers are shown. CP, Cortical plate. ***A***, Sagittal slice of the primary visual cortex (V1) at P4 showing *crym* (magenta) and *id2* (green) mRNAs labeled by FISH. ***A1***, Low-magnification photograph. ***A2–A4***, High-magnification photographs of the boxed region in ***A1*** showing *id2* mRNA (***A2***), *crym* mRNA (***A3***), and both (***A4***). Arrows indicate cells expressing both *id2* and *crym*. Thickness of the slice was 30 μm. ***B***, Coronal slice of the V1 of a P4 *Crym*-BAC-EGFP brain showing EGFP protein (green) labeled by immunohistochemistry (IHC) and *crym* mRNA (magenta) labeled by FISH. ***B1***, Low-magnification photograph. ***B2–B4***, High-magnification photographs of the boxed region in ***B1*** showing EGFP protein (***B2***), *crym* mRNA (***B3***), and both (***B4***). Arrows indicate cells expressing both EGFP protein and *crym* mRNA. Open arrowhead indicates a cell expressing *crym* mRNA but not EGFP protein. Thickness of the slice was 30 μm. ***C***, Coronal slice of the V1 of a P23 *Crym*-BAC-EGFP brain showing EGFP protein (green) labeled by IHC and subcerebral projection neurons (magenta) retrogradely labeled with CTB594 injected into the pons-midbrain junction. ***C1***, Low-magnification photograph. ***C2–C4***, High-magnification photographs of the boxed region in ***C1***, showing EGFP protein (***C2***), CTB594 (***C3***), and both (***C4***). Arrows indicate cells labeled for both EGFP protein and CTB594. Open arrowhead indicates a cell labeled for CTB594 but not for EGFP protein. Thickness of the slice was 100 μm. ***D***, Coronal slice of the V1 of a P78 *Crym*-BAC-EGFP brain showing EGFP (green) labeled by IHC and callosal projection neurons (magenta) retrogradely labeled with CTB594 injected into the contralateral cortex. ***D1***, Low-magnification photograph. ***D2–D4***, High-magnification photographs of the boxed region in ***D1*** showing EGFP protein (***D2***), CTB594 (***D3***), and both (***D4***). Arrowheads indicate cells labeled for EGFP but not for CTB594. Thickness of the slice was 100 μm. Scale bars: (in ***D1***) ***A1***, ***B1***, ***C1***, and ***D1***, 100 μm; (in ***D4***) for other panels, 50 μm. ***E–H,*** Brain slicing to obtain slices containing the binocular region of the *Crym*-BAC-EGFP mice. ***E***, Schematic representation of the mouse visual pathway. Blue indicates the left eye (L), the optic nerve, the thalamocortical axons conveying information from the left eye, and the monocular zone specific to the left eye. Orange indicates those for the right eye (R), and yellow denotes the binocular region. Single-eye visual stimulation was applied by closing the right eye (cross) while keeping the left eye open to receive light (arrow). Black dotted line indicates the approximate position of the parasagittal slice shown in ***G***. The primary visual cortex (V1) and the lateral secondary visual cortex (V2L) are indicated. ***F***, Schematic illustration of slicing to prepare slices for periodicity analysis. Brains were sliced in the orientation shown by the purple line. Black vertical line denotes the coronal plane. ***G***, Parasagittal brain slice of the left hemisphere of a P50 *Crym*-BAC-EGFP mouse given single-eye visual stimulation to the left eye showing EGFP (green) and c-Fos (magenta) proteins labeled by IHC. Asterisk indicates the position where EGFP is expressed in layer V of the binocular region. Thickness of the slice was 100 μm. Two white lines indicate the approximate position and orientation of coronal slices (see below). ***G1–G2***, Low-magnification photograph. Cx, Cerebral cortex; H, hippocampus; A, anterior; P, posterior. Scale bar, 500 μm. ***G3–G5***, High-magnification photograph of the boxed region in ***G1–G2*** showing EGFP protein (***G3***), c-Fos protein (***G4***), and both (***G5***). V1, Primary visual cortex; S1, Primary somatosensory cortex; V and VI, layers V and VI, respectively; dashed line, approximate border between V1 and S1. Scale bar, 200 μm. ***H***, Coronal brain slice of a P28 *Crym*-BAC-EGFP mouse given single-eye visual stimulation showing EGFP (green) and c-Fos (magenta) proteins labeled by IHC. The slice was approximately at the position indicated by the asterisk in ***G*** and approximately parallel to the white lines in ***G***. Arrowhead indicates the binocular region ipsilateral to the stimulated eye. The same slice as shown in Figure 11*B* and *C*. Scale bar, 500 μm.

Fig. 10*E*). Therefore, the periodic arrangement was not observed when all cell types in layer V were incorporated.

Correlated c-Fos expression in single repeating units under visual stimulation

We investigated whether neurons in single repeating units show similar neuronal activity. For this purpose, we examined the binocular region in the visual cortex, where subcerebral projection neurons labeled with EGFP showed a periodic arrangement in adult *Crym*-BAC-EGFP mice (see above). In the binocular region, most neurons respond to both eyes, and individual neurons have different selectivity between the contralateral and ipsilateral eyes (Hübener, 2003). Therefore, we examined whether neuronal activity induced by single-eye visual stimulation is similar among neurons within single repeating units. For this, we applied uniform white light to single eyes (Fig. 11*A*) of *Crym*-BAC-EGFP mice and investigated neuronal activity. Because extracellular electrophysiological recording typically has insufficient spatial resolution to discriminate neurons in adjacent repeating units and *in vivo* Ca^{2+} imaging is difficult in layer V, we examined activity-induced c-Fos protein expression to investigate neuronal activity (Sagar et al., 1988; Kaczmarek and Chaudhuri, 1997; Farivar et al., 2004; Yassin et al., 2010) (Fig. 11*B*,*C*). Subcerebral projection neurons were labeled by EGFP expression in layer V and grouped into single repeating units by analyzing the periodic arrangement (Fig. 11*D*; Materials and Methods).

We determined whether c-Fos is expressed randomly among EGFP(+) cells (Fig. 11*E*, left) or whether its expression is correlated within single repeating units, i.e., whether c-Fos tends to be expressed in EGFP(+) cells in the same repeating units (Fig. 11*E*, right). For this purpose, we investigated the following question: when an EGFP(+) cell (reference cell) is c-Fos(+), what is the probability that a neighboring EGFP(+) cell (target cell) is also c-Fos(+)? We determined this probability [*P*(c-Fos)] separately

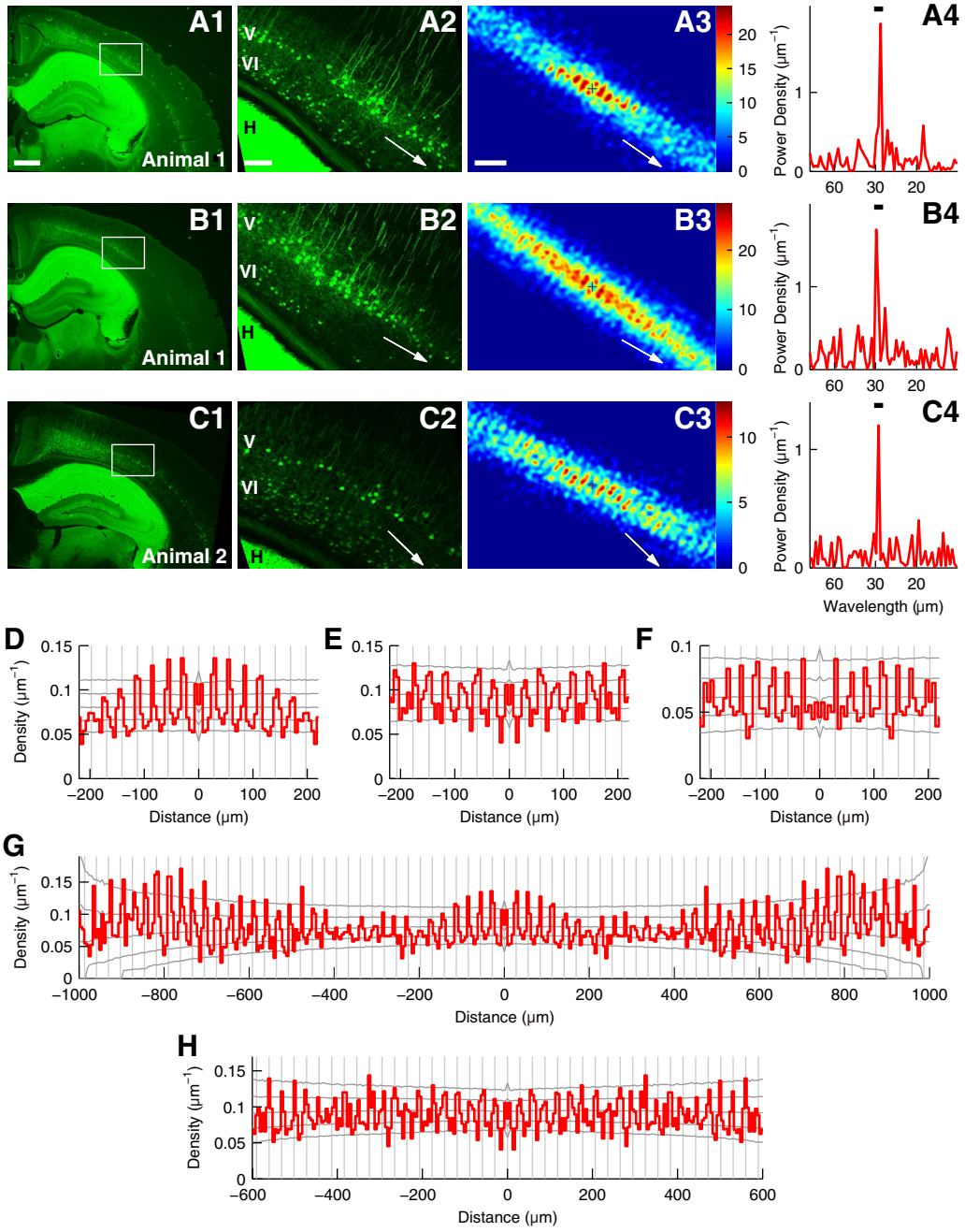

Figure 8. Periodic arrangement of EGFP(+) cells in the visual cortex of adult *Crym*-BAC-EGFP mice. ***A***, Analysis of a coronal slice of the visual cortex of a P41 *Crym*-BAC-EGFP mouse stained for EGFP protein. ***A1***, Low-magnification photograph. Scale bar, (in ***A1***) ***A1***, ***B1***, and ***C1***, 500 μm. ***A2***, High-magnification photograph of the area indicated by a rectangle in ***A1***. This area includes the binocular region, and it was used for periodicity analysis. White arrow denotes the orientation of periodicity. ***H***, Hippocampus; V and VI, layers V and VI, respectively, for ***A2***, ***B2***, and ***C2***. Scale bar, (in ***A2***) ***A2***, ***B2***, and ***C2***, 100 μm. ***A3***, Histogram of relative positions of EGFP(+) cells in layer V. The origin is shown by the plus sign, and the number of cells is shown in color. The histogram was smoothed with the Gaussian function ($\sigma = 6$ μm). White arrow denotes the orientation of periodicity. Scale bar, (in ***A3***) ***A3***, ***B3***, and ***C3***, 100 μm. ***A4***, Power spectrum of the distribution of EGFP(+) cells in layer V prepared for the orientation of periodicity. The peak wavelength = 28.2 μm. Bar indicates the wavelength range for significance analysis (27.5–30.5 μm). $p < 0.0001$. ***B***, Analysis of another slice from the same mouse as in ***A***. $\sigma = 6$ μm in ***B3***. The peak wavelength in ***B4*** = 29.8 μm. The wavelength range is 27.5–30.5 μm. $p = 0.0007$. ***C***, Analysis of a slice from another mouse at P35. $\sigma = 6$ μm in ***C3***. The peak wavelength in ***C4*** = 29.0 μm. The wavelength range is 27.5–30.5 μm. $p = 0.0026$. ***D–F***, Autocorrelograms of the positions of EGFP(+) cells in layer V in slices analyzed in ***A–C***. Autocorrelograms were prepared for the orientation of periodicity. Gray vertical lines are placed every 28.2, 29.5, and 29.0 μm, respectively. Gray lateral lines show the highest 2.5%, the highest 15.9%, the median, the lowest 15.9%, and the lowest 2.5% of autocorrelograms calculated for random surrogates. ***G***, ***H***, Identical autocorrelograms as in ***D*** and ***E***, shown for longer distance.

for target cells located within repeating units containing reference cells (Fig. 11*F*, left, indicated by an arrow with a solid arrowhead) and for target cells located within other repeating units, such as repeating units adjacent to repeating units containing reference cells (Fig. 11*F*, left, indicated by arrows with open arrowheads). If c-Fos expression is random, the probability that an EGFP(+) cell is c-Fos(+) is unrelated to neighboring cells, and therefore, P(c-Fos) will be similar at all relative positions (Fig. 11*F*, right, indicated by a black line). Under this hypothesis, i.e., random expression, P(c-Fos) can be estimated theoretically (Fig. 11*F*, right, P_{Rand}, indicated by the blue line). In contrast, if c-Fos tends to be expressed in the same repeating units, when an

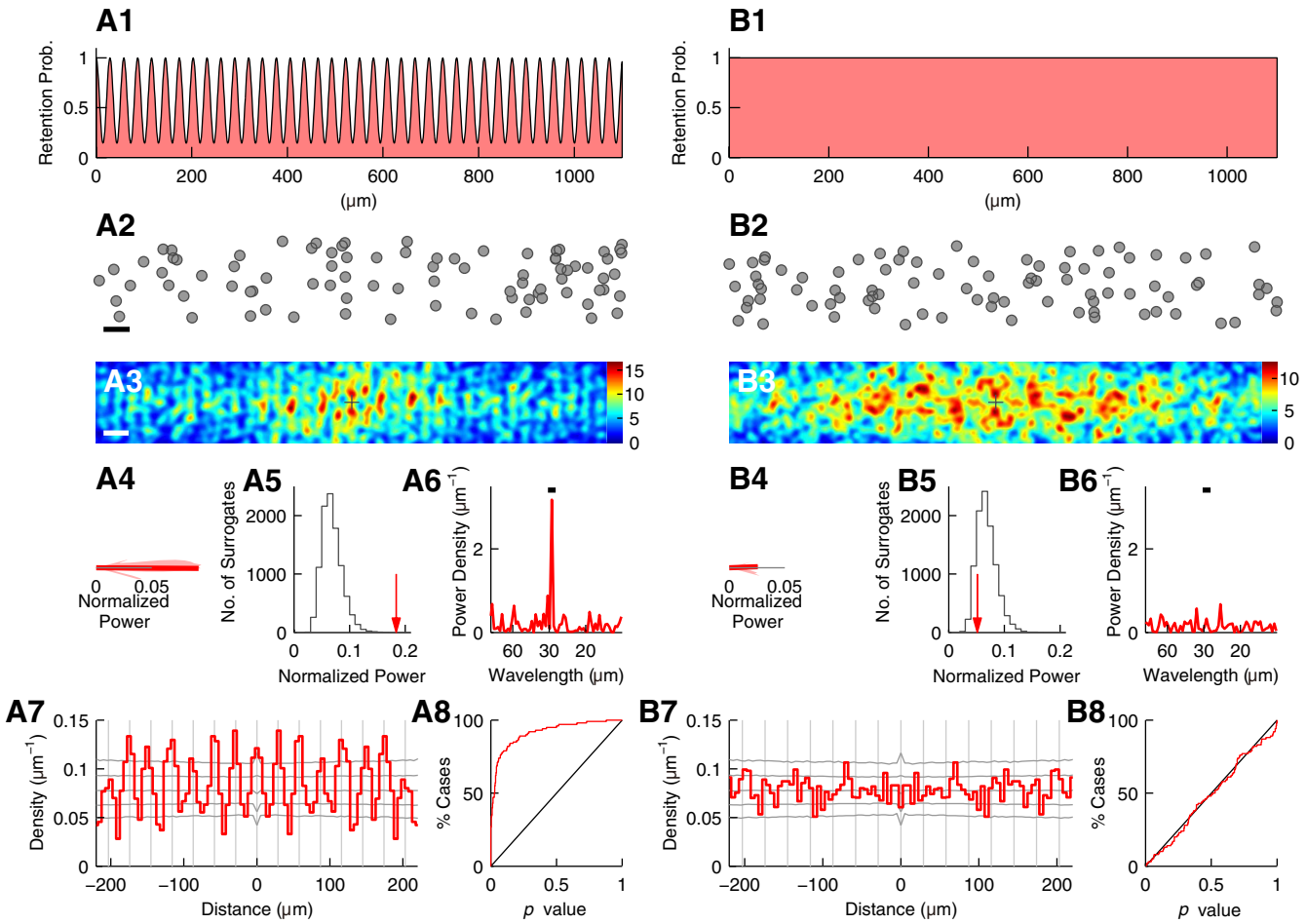

Figure 9. Periodicity analysis of simulated data. ***A***, Analysis of simulated data with periodicity. ***A1***, Probability to retain randomly placed cells. Probability curve is a sinusoid with a wavelength of 29 μm. The probabilities at the peaks and troughs are 1 and 1/7, respectively. ***A2***, An example set of cells generated according to the probability in ***A1***. In the radial orientation, cells are randomly distributed across 150 μm. Scale bar, 50 μm. Note that periodicity is not apparent. ***A3–A7***, Histogram of relative positions, normalized power, significance test, power spectrum, and autocorrelogram as shown in Figure 3, respectively. Scale bar, 50 μm; $\sigma = 6$ μm (in ***A3***). In ***A4–A6***, the wavelength range is 27.5–30.5 μm. In ***A5***, the number of surrogates is 10,000. $p < 0.0001$. In ***A7***, gray vertical lines are placed every 29.0 μm. ***A8***, Cumulative histogram of p values calculated for 100 simulated datasets. ***B***, The same analysis performed for simulated data without periodicity.

EGFP(+) cell is c-Fos(+), other EGFP(+) cells in the same repeating units will be c-Fos(+) more frequently than expected under random expression. In this case, P(c-Fos) at repeating units containing reference cells will be higher than that expected under random expression (Fig. 11*F*, right, indicated by a red line).

We calculated P(c-Fos) using all the 16 slices that showed significant periodicity [833 EGFP(+) cells, comprising 173 EGFP(+)c-Fos(+) and 660 EGFP(+)c-Fos(−) cells; 16 slices, 9 mice]. At repeating units containing reference cells, P(c-Fos) was significantly higher than expected under random expression (Fig. 11*G*; $^{***}p = 0.0001$). In contrast, for adjacent and second adjacent repeating units, P(c-Fos) was not significantly higher than expected under random expression (Fig. 11*G*; $p = 0.104$ and 0.098, respectively). Therefore, c-Fos expression was significantly correlated within single repeating units but not among adjacent units.

To further confirm the correlation, we performed the analysis at a higher spatial resolution. Because the above result suggests that c-Fos expression is correlated specifically within single repeating units, a higher spatial resolution would reveal radially extended correlation specifically within single repeating units. To test this prediction, we first calculated P(c-Fos) at various tangential distances relative to reference cells at 10 μm resolution (Fig. 11*H*, left). P(c-Fos) calculated for target cells located within repeating units containing reference cells is indicated by a thick red line in the right panel in Figure 11*H*. When target cells were within 5 μm in the tangential orientation from reference cells, P(c-Fos) was 49.6% (Fig. 11*H*, right; $^{****}p < 0.0001$, indicated by the thick red line); this value is more than twice of P_{Rand} (Fig. 11*H*, right, 24.3%; indicated by the blue line). Similarly, when the tangential distance between target and reference cells was 5–15 μm, P(c-Fos) was significantly higher than expected under the random distribution (Fig. 11*H*, right; $p = 0.041$, indicated by the thick red line).

We then performed the analysis in the radial orientation for target cells located within repeating units containing reference cells. We limited the analysis to target cells located within 5 μm in the tangential orientation from reference cells and calculated P(c-Fos) at various radial positions relative to reference cells (Fig. 11*I*, left). The result showed that P(c-Fos) was significantly higher than expected under random expression up to a radial range of ± 60 μm (Fig. 11*I*, right).

We performed a similar analysis for target cells located outside repeating units containing reference cells. In contrast to the above results, no significant correlation was observed when we analyzed in the tangential orientation (Fig. 11*H*, right, indicated by the thin red lines). We confirmed that these results did not

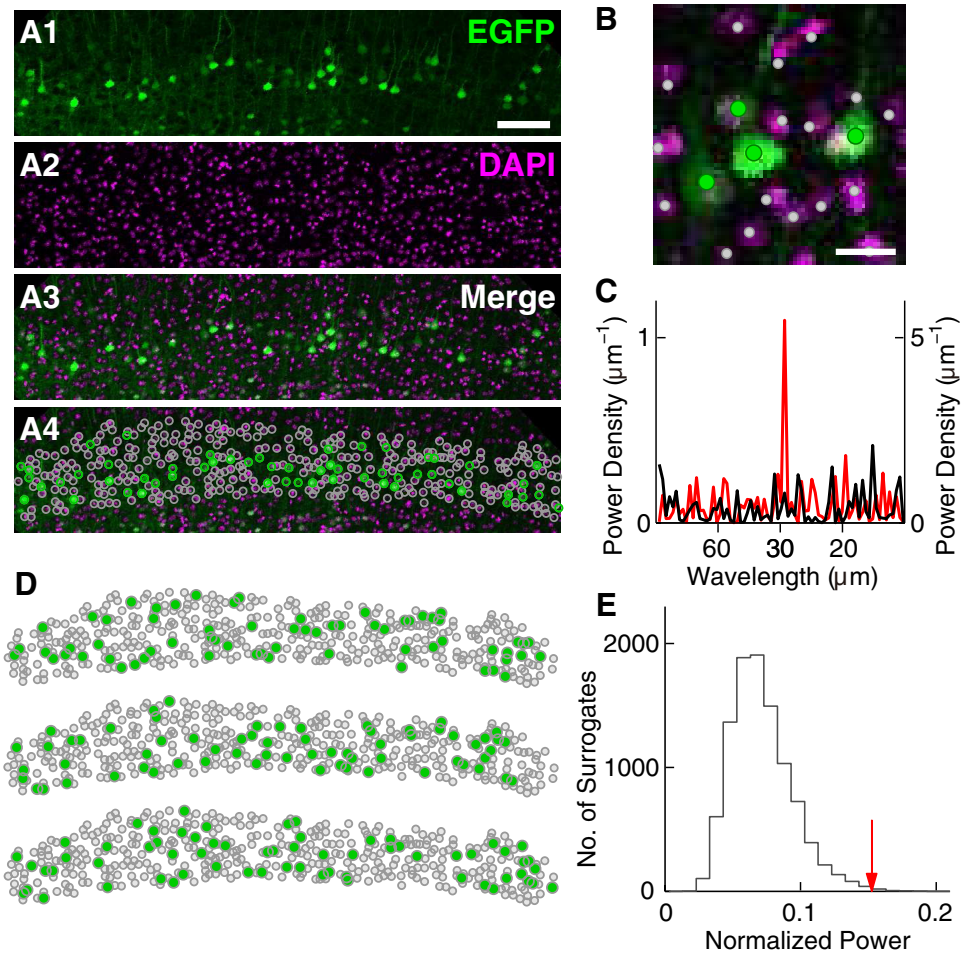

Figure 10. Periodicity analysis with all cell types in layer V. ***A***, The same slice as shown in Figure 8*C2*. A coronal slice of the visual cortex of a P35 *Crym*-BAC-EGFP mouse showing EGFP protein labeled by immunohistochemistry (***A1***), DAPI staining of nuclei (***A2***), and both (***A3*** and ***A4***). In ***A4***, the positions of EGFP(+) and EGFP(−) nuclei in layer V are shown by green and gray open circles, respectively. Scale bar, 100 μm. ***B***, High-magnification photograph of ***A4***. Cells are marked similarly to ***A4***, except that markers are solid circles. Scale bar, 20 μm. ***C***, Red, Power spectrum of the cell position histogram of EGFP(+) cells in ***A4*** prepared for the orientation of periodicity. The same graph as shown in Figure 8*C4*. The vertical axis is on the left. Black, Power spectrum of the positions of all cells, i.e., EGFP(+) cells and EGFP(−) nuclei in ***A4***, measured in the same orientation as that used for the red curve. The vertical axis is on the right. ***D***, Three surrogate datasets generated by randomly selecting surrogate EGFP(+) cells among all cells labeled in ***A4***. The number of surrogate EGFP(+) cells was the same as that of the real EGFP(+) cells in A4. ***E***, Red arrow, Normalized power calculated for EGFP(+) cells in the real data. Gray, Histogram of normalized power calculated for 10,000 surrogates generated as shown in ***D***. Among the 10,000 surrogates, only 16 had normalized power larger than that of the real data.

depend on the details of the analysis (Fig. 11*J*; Materials and Methods). Therefore, as expected, the high-resolution analysis showed that c-Fos expression was correlated in a radially extended area relative to reference cells ($\pm$15 and $\pm$60 μm in the tangential and radial orientations, respectively), specifically within single repeating units (Fig. 11*K*). Because the thickness of layer V is only ~150 μm in the binocular region (Fig. 8*A*–C), this result suggests that the radial correlation extended across nearly the entire thickness of layer V.

Hence, under single-eye stimulation, c-Fos expression was significantly correlated within single repeating units but not among adjacent units, suggesting that neuronal activity leading to c-Fos expression is similar among neurons in the same repeating units but not among those in adjacent units.

Discussion

Our results indicate that the distribution of subcerebral projection neurons, a major pyramidal neuron subtype in neocortical layer V, is not random but significantly periodic in the tangential orientation. The wavelength of periodicity was ~30 μm. This periodic organization was observed in the visual and somatosensory cortex, suggesting that it is a common organizational characteristic across cortical areas. Under single-eye visual stimulation, activity-induced c-Fos expression in the binocular region was correlated among neurons within single repeating units but not adjacent units. These results suggest that neocortical layer V has stereotyped, periodic tangential organization: subcerebral projection neurons are located periodically, and neuronal activity leading to c-Fos expression is similar among neurons in single repeating units (Fig. 12).

Structure of periodic organization

Although periodic organization commonly exists in different cortical areas and at different ages, structural differences were observed. First, the wavelengths differed: the wavelengths were ~23 μm in the P4 posterior visual cortex, ~33 μm in the P9 somatosensory cortex, and ~30 μm in the adult visual cortex around the binocular region. Second, the distribution of neurons within each unit differed. In the posterior visual cortices of young mice, *id2*(+) cells were relatively dense and often formed radial contiguous clusters, in which the cells were in contact with other cells. Conversely, in the P9 somatosensory and adult visual cortices, subcerebral projection neurons (labeled by *id2* and *Crym*-

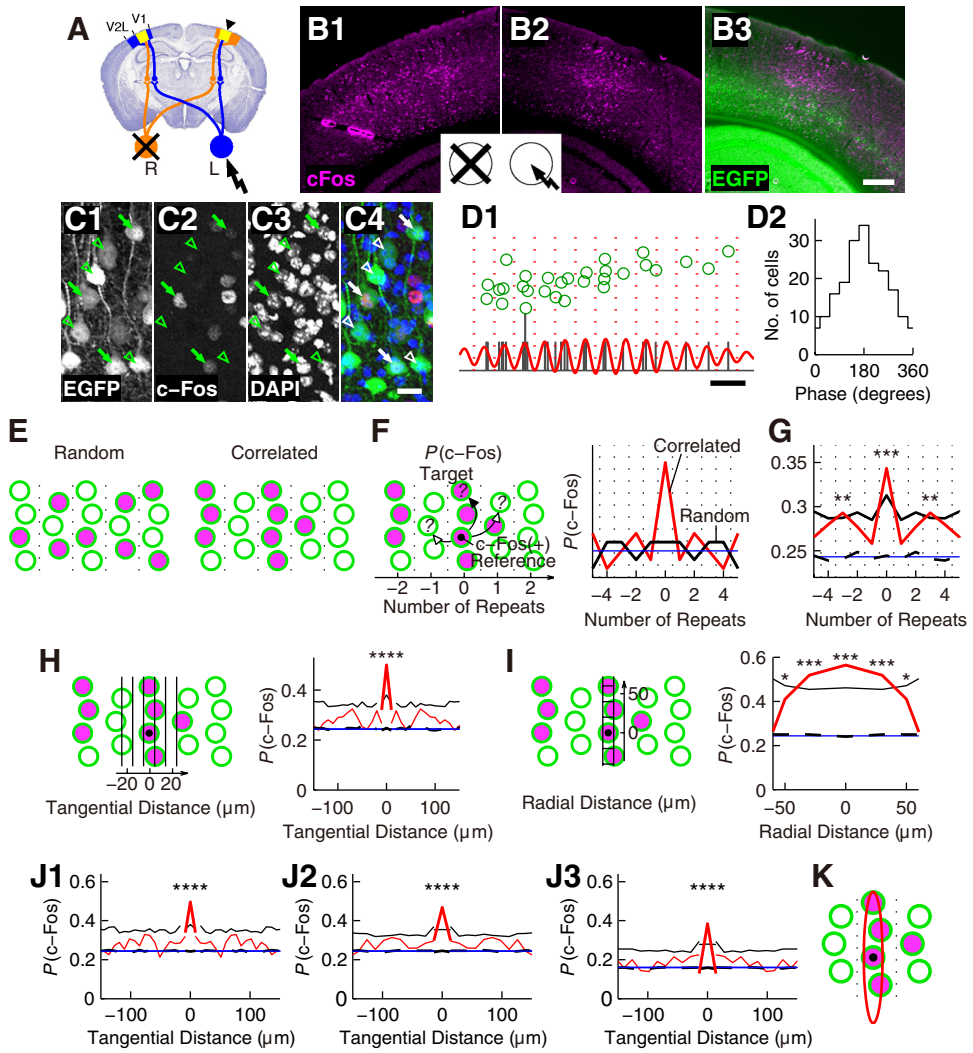

Figure 11. Correlation analysis of c-Fos expression. ***A***, Schematic representation of the mouse visual pathway as shown in Figure 7*E* on a coronal slice. ***B–C***, c-Fos protein expression in the visual cortex of a P28 *Crym*-BAC-EGFP mouse induced by single-eye visual stimulation to the left eye. ***B***, Low-magnification photographs showing c-Fos (magenta) and EGFP (green) proteins labeled by IHC. ***B1–B2***, The right (***B1***) and left (***B2***) hemispheres are shown. Open and closed eyes are shown schematically as in ***A***. Note the asymmetry of c-Fos expression between the two hemispheres. The area that showed c-Fos expression in ***B2*** is the left binocular region. ***B3***, The same slice as ***B2*** simultaneously visualized for c-Fos and EGFP. Scale bar, 300 μm. ***C***, High-magnification photographs of layer V in ***B3*** showing EGFP (***C1***), c-Fos (***C2***), DAPI staining of nuclei (***C3***), and merged image (***C4***; green, EGFP; red, c-Fos; blue, DAPI). Arrows indicate EGFP(+)c-Fos(+) cells, and open arrowheads indicate EGFP(+)c-Fos(−) cells. Scale bar, 20 μm. ***D***, Grouping cells into repeating units. ***D1***, Green circles represent EGFP(+) cells in a part of the slice shown in Figure 8*A2*. The orientation of periodicity was set to be horizontal. The cell position histogram is shown in black. Red line is the bandpass filtered histogram (wavelength range = 27.5–30.5 μm). The vertical scale and the vertical position of the red line were adjusted to overlap the histogram. Red dotted lines represent the borders located at troughs of the red line. Scale bar, 50 μm. ***D2***, Phase histogram of EGFP(+) cells in slices shown in Figure 8*A2* and *B2*. ***E–J***, Analysis of correlation in c-Fos expression. ***E***, Schematic illustration of random (left) and correlated (right) c-Fos expression. Only EGFP(+) subcerebral projection neurons are shown. Green open circles are EGFP(+)c-Fos(−) cells, while green circles filled with magenta are EGFP(+)c-Fos(+) cells. Dotted lines are borders between repeating units. ***F***, Left, Schematic illustration of the definition of *P*(c-Fos). Black dot denotes an EGFP(+)c-Fos(+) cell used as a reference cell. *P*(c-Fos) was calculated for target cells located within repeating units containing reference cells (arrow with solid arrowhead) or for target cells located within other repeating units such as those adjacent to repeating units containing reference cells (arrows with open arrowheads). Right, *P*(c-Fos) expected under random (black) or correlated (red) expression. Blue line denotes P_{Rand}. ***G***, Red, *P*(c-Fos) calculated with data obtained from nine mice. $^{**}p < 0.01$; $^{***}p = 0.0001$. Blue, P_{Rand}. Black solid and black dashed lines indicate the highest 1% and the median of *P*(c-Fos) calculated with surrogate data that have random c-Fos expression, respectively. ***H***, Analysis at high spatial resolution. Left, Arrangement of bins to calculate *P*(c-Fos) at positions relative to reference EGFP(+)c-Fos(+) cells (black dot). Right, *P*(c-Fos) calculated for target cells located within repeating units containing reference cells (thick red line) and for target cells located within other repeating units (thin red line). $^{****}p < 0.0001$. Black solid and black dashed lines are results of surrogate data calculated separately for the two cases and shown as in ***G***. Blue line denotes P_{Rand}. ***I***, Analysis in the radial orientation. Left, Arrangement of bins. Black dot denotes a reference EGFP(+)c-Fos(+) cell. Right, Result obtained for target cells located within repeating units containing reference cells, shown as in ***G***. $^{*}p < 0.05$; $^{***}p = 0.0002$ and 0.0006 for the central and the adjacent bins, respectively. ***J***, Robustness tests shown as in the right panel in ***H***. ***J1–J2***, The same analyses as shown in ***H*** was performed using bins with widths of 8.5 μm (***J1***) and 14 μm (***J2***). ***J3***, The same analyses as shown in ***J2*** was performed using 121 EGFP(+)c-Fos(+) cells that showed relatively strong c-Fos expression among the 173 EGFP(+)c-Fos(+) cells used in ***J2***. ***K***, Schematic illustration of the correlation at high resolution. Within a single repeating unit, c-Fos expression was correlated across approximately ±15 and ±60 μm in the tangential and radial orientations, respectively (red ellipse), relative to reference EGFP(+)c-Fos(+) cells (black dot).

BAC-EGFP, respectively) were sparse and often did not form contiguous radial clusters.

Periodicity was not detected when all cell types in layer V were incorporated (Figs. 2C1, 10). However, this result does not exclude the possibility that cell types other than subcerebral projection neurons have periodicity. Even if other cell types have periodicity, their incorporation could weaken the observed periodicity if their phases were different from those of subcerebral projection neurons. In addition, compared with subcerebral projection neurons, which are a major cell type in layer V and include

the largest pyramidal neurons (Molnár and Cheung, 2006; Molyneaux et al., 2007), other cell types could be smaller or more dispersed, making clustering and periodicity less apparent. Therefore, more analyses are necessary to determine whether cell types other than subcerebral projection neurons have periodicity.

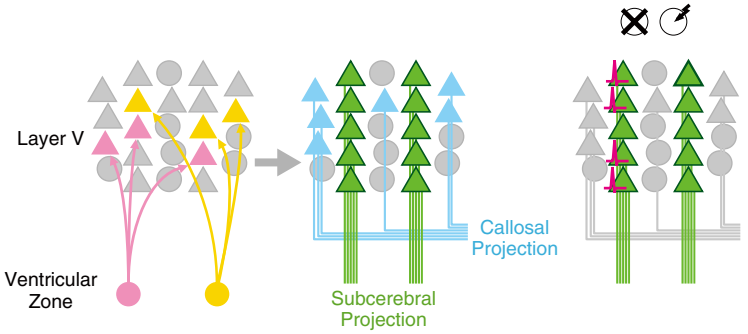

Figure 12. Summary of the study. Left, During corticogenesis, cortical progenitor cells (red and yellow circles) generate pyramidal neurons (red and yellow triangles). Pyramidal neurons of different lineages are located at positions intermingled in layer V. Gray circles represent inhibitory interneurons and glial cells, and gray triangles represent pyramidal neurons of other lineages. Middle, Subcerebral projection neurons (green) of different lineages form single repeating units, which are arranged periodically. Callosal projection neurons are shown in cyan. Right, Under single-eye visual stimulation (top), subcerebral projection neurons in the same repeating units show similar neuronal activities that lead to c-Fos expression (bottom).

Relationship to previously characterized neocortical structures

It has been unclear whether the mouse binocular region has substructures (Hübener, 2003). Our results suggest that the mouse binocular region has functional substructures, at least for subcerebral projection neurons in layer V. The width of ocular dominance columns in cats and monkeys is typically ~500 μm (Mountcastle, 1997); hence, if periodic organization exists in these cortical columns, a column would contain at least dozens of repeating units.

In addition to their subcortical targets, subcerebral projection neurons innervate neighboring neurons in neocortical layer V. In the primary visual cortex in mice, neurons innervated by corticotectal neurons, a subset of subcerebral projection neurons, are located at nonrandom positions relative to the corticotectal neurons innervating them (Kozloski et al., 2001). Therefore, neurons locally connected to repeating units may have a regular arrangement relative to repeating units.

A recent analysis showed that pyramidal neurons in layer II/III preferentially connect with neurons in layer V that are clonally related (Yu et al., 2009). This selective connection would not provide specific input to single repeating units, because neurons within single repeating units are generally not clonally closer than those within neighboring units. Instead, such selectivity may provide a selective connection to specific subsets of neurons within repeating units.

Classical anatomy has described several radial structures in the neocortex. Apical dendrites of layer V pyramidal neurons tend to form bundles (Peters and Walsh, 1972; Peters and Sethares, 1991, 1996; Jones, 2000; Rockland and Ichinohe, 2004; DeFelipe, 2005; Innocenti and Vercelli, 2010). However, in *Crym*-BAC-EGFP mice, many EGFP(+) cells did not appear to form distinct dendritic bundles (Fig. 7*B–D*). When cells in the primate neocortex are visualized using Nissl staining, they are often arranged in vertically aligned columns (Schlaug et al., 1995; Buxhoeveden et al., 2000; Jones, 2000; Rockland and Ichinohe, 2004; DeFelipe, 2005). We did not find this structure in mice because periodicity was not detected when all cell types were incorporated (Figs. 2*C*1,10). In primates, a type of interneuron, double bouquet cells, forms vertical axonal bundles positioned with regular spacing (DeFelipe et al., 1990); however, it is unclear whether rodents have this structure (Yáñez et al., 2005). Therefore, further analysis is required to determine the relationship between these anatomical structures and periodic organization.

Developmental mechanisms

As our clonal analysis indicated that single repeating units are not generated by radial alignment of sibling neurons (Fig. 12), their development may involve intercellular interactions. During corticogenesis, newborn pyramidal neurons show tangential dispersion as well as radial migration. This tangential dispersion depends on Eph receptor A and ephrin-A (Torii et al., 2009), suggesting that tangential distribution is regulated by intercellular signaling. Moreover, subcerebral projection neurons regulate the distribution of inhibitory interneurons (Lodato et al., 2011). These or other intercellular signaling mechanisms may be involved in the construction of periodic organization. Another possible mechanism is synchronized neuronal activity among radially aligned neurons in the developing neocortex (Yuste et al., 1992; Dupont et al., 2006; Khazipov and Luhmann, 2006). Because these activities synchronize neurons within tens of micrometers in the tangential orientation, they may be involved in the formation of periodic organization.

Functional implications

In the neocortex, functional clustering and neuronal interactions have been observed among neurons located within tens of micrometers in the tangential orientation. Such organization is found in multiple cortical areas including the visual (Hubel and Wiesel, 1974, 1977; Ohki et al., 2006; Kara and Boyd, 2009), somatosensory (Bruno et al., 2003; Andermann and Moore, 2006), motor (Amirikian and Georgopoulos, 2003; Georgopoulos et al., 2007; Dombeck et al., 2009; Komiyama et al., 2010), and frontal cortex (Opris et al., 2011). Our results suggest that cortical functions performed within tens of micrometers in the tangential orientation may be processed by local circuits with a periodic neuronal distribution. One possible benefit of periodic organization is to precisely provide the same sets of neuronal subtypes at different tangential positions in the neocortex.

Neurons in single repeating units showed correlated c-Fos expression. Although c-Fos expression is generally well correlated with neuronal activity (Sagar et al., 1988; Kaczmarek and Chaudhuri, 1997; Farivar et al., 2004; Yassin et al., 2010), it will be necessary in the future to determine how precisely c-Fos expression correlates with action potentials under our experimental conditions. Nevertheless, the correlated c-Fos expression suggests that neurons in single repeating units have similar neuronal activity, and therefore have related functions. Because repeating units are found in multiple cortical areas, their functions may be similar across different cortical areas.

Subcerebral projection neurons are thought to play a major role in information processing in layer V (Le Bé et al., 2007) and constitute an important class of neurons that send information out of the neocortex. For example, corticospinal motor neurons, a subset of subcerebral projection neurons sending projections to the spinal

cord, form the basis of voluntary movement (Lemon, 2008). Therefore, our results indicate that a major output system of the neocortex is composed of periodically arranged neurons. One possibility is that neurons in a single repeating unit may function as a single output unit that sends out related information.

It has been unclear whether the rodent neocortex has columnar organization other than barrels, which are located in the somatosensory area and have a typical diameter of 200 μm. Our results indicate that the mouse neocortex has columnar micro-organization at the scale of tens of micrometers, at least in layer V of the visual and somatosensory cortex. In addition, previous observations of functional clustering and neuronal interactions among neurons located within tens of micrometers in the tangential orientation have led to the hypotheses that the cortical circuit is composed of building blocks that are radial neuronal clusters with a diameter of tens of micrometers ("minicolumn" hypothesis) (Hubel and Wiesel, 1974, 1977; Kaas et al., 1981; McCasland and Woolsey, 1988; Tommerdahl et al., 1993; Favorov and Kelly, 1994; Kohn et al., 1997; Mountcastle, 1997; Buxhoeveden and Casanova, 2002; Mountcastle, 2003). Although this structure was originally proposed for higher mammals, our results suggest that the mouse neocortex has a similar structure, at least for a subtype of pyramidal neurons in layer V. One possibility is that a single repeating unit of subcerebral projection neurons is a component of a single elementary unit of the neocortical circuit. This hypothesis needs to be examined in the future.

Conclusion

In summary, our results demonstrate that the mouse neocortex has a periodic functional micro-organization composed of a major neuronal subtype in layer V. In the visual and somatosensory areas, subcerebral projection neurons have a periodic arrangement with a typical wavelength of 30 μm. Under specific visual stimulation, neuronal activity leading to c-Fos expression is similar among neurons in the same repeating units. This periodic organization may underlie the function of local cortical circuits and could provide an opportunity to further identify stereotypy in the neocortex.

References

Amirikian B, Georgopoulos AP (2003) Modular organization of directionally tuned cells in the motor cortex: is there a short-range order? Proc Natl Acad Sci U S A 100:12474–12479.

Andermann ML, Moore CI (2006) A somatotopic map of vibrissa motion direction within a barrel column. Nat Neurosci 9:543–551.

Anthony TE, Klein C, Fishell G, Heintz N (2004) Radial glia serve as neuronal progenitors in all regions of the central nervous system. Neuron 41:881–890.

Arlotta P, Molyneaux BJ, Chen J, Inoue J, Kominami R, Macklis JD (2005) Neuronal subtype-specific genes that control corticospinal motor neuron development in vivo. Neuron 45:207–221.

Bruno RM, Khatri V, Land PW, Simons DJ (2003) Thalamocortical angular tuning domains within individual barrels of rat somatosensory cortex. J Neurosci 23:9565–9574.

Buxhoeveden DP, Casanova MF (2002) The minicolumn hypothesis in neuroscience. Brain 125:935–951.

Buxhoeveden DP, Switala AE, Roy E, Casanova MF (2000) Quantitative analysis of cell columns in the cerebral cortex. J Neurosci Methods 97:7–17.

Danielian PS, Muccino D, Rowitch DH, Michael SK, McMahon AP (1998) Modification of gene activity in mouse embryos in utero by a tamoxifen-inducible form of Cre recombinase. Curr Biol 8:1323–1326.

DeFelipe J (2005) Reflections on the structure of the cortical minicolumn. In: Neocortical modularity and the cell minicolumn (Casanova MF, ed), pp 57–92. New York: Nova Science.

DeFelipe J, Hendry SH, Hashikawa T, Molinari M, Jones EG (1990) A microcolumnar structure of monkey cerebral cortex revealed by immunocytochemical studies of double bouquet cell axons. Neuroscience 37:655–673.

Dombeck DA, Graziano MS, Tank DW (2009) Functional clustering of neurons in motor cortex determined by cellular resolution imaging in awake behaving mice. J Neurosci 29:13751–13760.

Dupont E, Hanganu IL, Kilb W, Hirsch S, Luhmann HJ (2006) Rapid developmental switch in the mechanisms driving early cortical columnar networks. Nature 439:79–83.

Farivar R, Zangenehpour S, Chaudhuri A (2004) Cellular-resolution activity mapping of the brain using immediate-early gene expression. Front Biosci 9:104–109.

Favorov OV, Kelly DG (1994) Minicolumnar organization within somatosensory cortical segregates: I. Development of afferent connections. Cereb Cortex 4:408–427.

Feng L, Heintz N (1995) Differentiating neurons activate transcription of the brain lipid-binding protein gene in radial glia through a novel regulatory element. Development 121:1719–1730.

Georgopoulos AP, Merchant H, Naselaris T, Amirikian B (2007) Mapping of the preferred direction in the motor cortex. Proc Natl Acad Sci U S A 104:11068–11072.

Hallen A, Cooper AJ, Jamie JF, Haynes PA, Willows RD (2011) Mammalian forebrain ketimine reductase identified as mu-crystallin; potential regulation by thyroid hormones. J Neurochem 118:379–387.

Hatten ME (1999) Central nervous system neuronal migration. Annu Rev Neurosci 22:511–539.

Hayashi S, McMahon AP (2002) Efficient recombination in diverse tissues by a tamoxifen-inducible form of Cre: a tool for temporally regulated gene activation/inactivation in the mouse. Dev Biol 244:305–318.

Holmgren C, Harkany T, Svennenfors B, Zilberter Y (2003) Pyramidal cell communication within local networks in layer 2/3 of rat neocortex. J Physiol 551:139–153.

Hubel DH, Wiesel TN (1974) Sequence regularity and geometry of orientation columns in the monkey striate cortex. J Comp Neurol 158:267–293.

Hubel DH, Wiesel TN (1977) Ferrier lecture. Functional architecture of macaque monkey visual cortex. Proc R Soc Lond B Biol Sci 198:1–59.

Hübener M (2003) Mouse visual cortex. Curr Opin Neurobiol 13:413–420.

Innocenti GM, Vercelli A (2010) Dendritic bundles, minicolumns, columns, and cortical output units. Front Neuroanat 4:11.

Jones EG (2000) Microcolumns in the cerebral cortex. Proc Natl Acad Sci U S A 97:5019–5021.

Kaas JH, Nelson RJ, Sur M, Merzenich MM (1981) Organization of somatosensory cortex in primates. In: The organization of the cerebral cortex (Schmitt FO, Worden FG, Adelman G, Dennis SG, eds), pp 237–261. Cambridge, MA: MIT.

Kaczmarek L, Chaudhuri A (1997) Sensory regulation of immediate-early gene expression in mammalian visual cortex: implications for functional mapping and neural plasticity. Brain Res Brain Res Rev 23:237–256.

Kara P, Boyd JD (2009) A micro-architecture for binocular disparity and ocular dominance in visual cortex. Nature 458:627–631.

Kee BL (2009) E and ID proteins branch out. Nat Rev Immunol 9:175–184.

Khazipov R, Luhmann HJ (2006) Early patterns of electrical activity in the developing cerebral cortex of humans and rodents. Trends Neurosci 29:414–418.

Kohn A, Pinheiro A, Tommerdahl MA, Whitsel BL (1997) Optical imaging in vitro provides evidence for the minicolumnar nature of cortical response. Neuroreport 8:3513–3518.

Komiyama T, Sato TR, O'Connor DH, Zhang YX, Huber D, Hooks BM, Gabitto M, Svoboda K (2010) Learning-related fine-scale specificity imaged in motor cortex circuits of behaving mice. Nature 464:1182–1186.

Kozloski J, Hamzei-Sichani F, Yuste R (2001) Stereotyped position of local synaptic targets in neocortex. Science 293:868–872.

Lasorella A, Stegmüller J, Guardavaccaro D, Liu G, Carro MS, Rothschild G, de la Torre-Ubieta L, Pagano M, Bonni A, Iavarone A (2006) Degradation of Id2 by the anaphase-promoting complex couples cell cycle exit and axonal growth. Nature 442:471–474.

Le Bé JV, Silberberg G, Wang Y, Markram H (2007) Morphological, electrophysiological, and synaptic properties of corticocallosal pyramidal cells in the neonatal rat neocortex. Cereb Cortex 17:2204–2213.

Lemon RN (2008) Descending pathways in motor control. Annu Rev Neurosci 31:195–218.

Lodato S, Rouaux C, Quast KB, Jantrachotechatchawan C, Studer M, Hensch

TK, Arlotta P (2011) Excitatory projection neuron subtypes control the distribution of local inhibitory interneurons in the cerebral cortex. Neuron 69:763–779.
McCasland JS, Woolsey TA (1988) High-resolution 2-deoxyglucose mapping of functional cortical columns in mouse barrel cortex. J Comp Neurol 278:555–569.
Molnár Z, Cheung AF (2006) Towards the classification of subpopulations of layer V pyramidal projection neurons. Neurosci Res 55:105–115.
Molyneaux BJ, Arlotta P, Menezes JR, Macklis JD (2007) Neuronal subtype specification in the cerebral cortex. Nat Rev Neurosci 8:427–437.
Mountcastle VB (1997) The columnar organization of the neocortex. Brain 120:701–722.
Mountcastle VB (2003) Introduction. Computation in cortical columns. Cereb Cortex 13:2–4.
Neuman T, Keen A, Zuber MX, Kristjansson GI, Gruss P, Nornes HO (1993) Neuronal expression of regulatory helix-loop-helix factor Id2 gene in mouse. Dev Biol 160:186–195.
Novak A, Guo C, Yang W, Nagy A, Lobe CG (2000) Z/EG, a double reporter mouse line that expresses enhanced green fluorescent protein upon Cre-mediated excision. Genesis 28:147–155.
Ohki K, Chung S, Kara P, Hübener M, Bonhoeffer T, Reid RC (2006) Highly ordered arrangement of single neurons in orientation pinwheels. Nature 442:925–928.
Opris I, Hampson RE, Stanford TR, Gerhardt GA, Deadwyler SA (2011) Neural activity in frontal cortical cell layers: evidence for columnar sensorimotor processing. J Cogn Neurosci 23:1507–1521.
Peters A, Sethares C (1991) Organization of pyramidal neurons in area 17 of monkey visual cortex. J Comp Neurol 306:1–23.
Peters A, Sethares C (1996) Myelinated axons and the pyramidal cell modules in monkey primary visual cortex. J Comp Neurol 365:232–255.
Peters A, Walsh TM (1972) A study of the organization of apical dendrites in the somatic sensory cortex of the rat. J Comp Neurol 144:253–268.
Rockland KS, Ichinohe N (2004) Some thoughts on cortical minicolumns. Exp Brain Res 158:265–277.
Rubenstein JL, Anderson S, Shi L, Miyashita-Lin E, Bulfone A, Hevner R (1999) Genetic control of cortical regionalization and connectivity. Cereb Cortex 9:524–532.
Sagar SM, Sharp FR, Curran T (1988) Expression of c-Fos protein in brain: metabolic mapping at the cellular level. Science 240:1328–1331.
Schlaug G, Schleicher A, Zilles K (1995) Quantitative analysis of the columnar arrangement of neurons in the human cingulate cortex. J Comp Neurol 351:441–452.
Silberberg G, Gupta A, Markram H (2002) Stereotypy in neocortical microcircuits. Trends Neurosci 25:227–230.
Tommerdahl M, Favorov O, Whitsel BL, Nakhle B, Gonchar YA (1993) Minicolumnar activation patterns in cat and monkey SI cortex. Cereb Cortex 3:399–411.
Torii M, Hashimoto-Torii K, Levitt P, Rakic P (2009) Integration of neuronal clones in the radial cortical columns by EphA and ephrin-A signalling. Nature 461:524–528.
Yáñez IB, Muñoz A, Contreras J, Gonzalez J, Rodriguez-Veiga E, DeFelipe J (2005) Double bouquet cell in the human cerebral cortex and a comparison with other mammals. J Comp Neurol 486:344–360.
Yassin L, Benedetti BL, Jouhanneau JS, Wen JA, Poulet JF, Barth AL (2010) An embedded subnetwork of highly active neurons in the neocortex. Neuron 68:1043–1050.
Yu YC, Bultje RS, Wang X, Shi SH (2009) Specific synapses develop preferentially among sister excitatory neurons in the neocortex. Nature 458:501–504.
Yuste R, Peinado A, Katz LC (1992) Neuronal domains in developing neocortex. Science 257:665–669.